

# Non-dissipative space-time $hp$ -discontinuous Galerkin method for the time-dependent Maxwell equations

M. Lilienthal<sup>a,c,\*</sup>, S.M. Schnepp<sup>b</sup>, T. Weiland<sup>c</sup>

<sup>a</sup>*Graduate School of Computational Engineering, Technische Universitaet Darmstadt, Dolivostrasse 15, 64293 Darmstadt, Germany*

<sup>b</sup>*ETH Zurich, Institute of Electromagnetic Fields (IFH), Gloriastrasse 35, 8092 Zurich, Switzerland*

<sup>c</sup>*Institut fuer Theorie Elektromagnetischer Felder, Technische Universitaet Darmstadt, Schlossgartenstrasse 8, 64289 Darmstadt, Germany*

---

## Abstract

A finite element method for the solution of the time-dependent Maxwell equations in mixed form is presented. The method allows for local  $hp$ -refinement in space and in time. To this end, a space-time Galerkin approach is employed. In contrast to the space-time DG method introduced in [1] test and trial space do not coincide. This allows for obtaining a non-dissipative method. To obtain an efficient implementation, a hierarchical tensor product basis in space and time is proposed. This allows to evaluate the local residual with a complexity of  $\mathcal{O}(p^4)$  and  $\mathcal{O}(p^5)$  for affine and non-affine elements, respectively.

---

## 1. Introduction

The accurate solution of large scale electromagnetic problems, where short wavelengths need to be resolved in large computational domains, remains a challenge. Examples include antenna design, broadband scattering problems or electrically large structures. Especially for problems, where dispersion errors dominate, high order methods have advantages. Furthermore, if  $hp$ -refinement is applied in a judicious way, it is possible to obtain exponential convergence, even for solutions, which are locally non-smooth [2]. This can lead to drastical savings in terms of degrees of freedom. In the past decade, there has been a lot of research on discontinuous Galerkin (DG) methods for Maxwell's equations, see e.g. [3, 4, 5]. The use of discontinuous finite element spaces, allows in a natural way for  $hp$ -refinement without the use of special transition elements as it is the case for continuous finite element methods [6, 7]. Often, DG methods are chosen for the spatial part of the discretization, whereas time is discretized

---

\*Corresponding Author

*Email addresses:* lilienthal@gsc.tu-darmstadt.de (M. Lilienthal), sascha.schnepp@ifh.ee.ethz.ch (S.M. Schnepp), thomas.weiland@temf.tu-darmstadt.de (T. Weiland)

with explicit time integrators. Due to the conditional stability of the resulting schemes, the time step size in this case is determined by the smallest element and also the degree of the approximating polynomials. Thus, the temporal resolution is dictated by stability, not by actual accuracy requirements. To overcome this problem, local time-stepping schemes [5, 8, 9] and locally implicit schemes [10, 11] have been proposed. For both approaches, good speedups on locally refined meshes are reported. However, refinement in time is necessary for stability, rather than accuracy requirements.

Another approach are space-time DG methods [1]. Since space and time are discretized simultaneously, *hp*-refinement in space and time can be introduced naturally. The space-time DG methods are unconditionally stable. Together with their high flexibility, these methods are well-suited for space-time adaptivity. However, many of the previously introduced space-time DG methods are dissipative. Dissipation may become an issue, especially for low approximation orders. In this paper we propose a space-time finite element method which is discontinuous with respect to the spatial directions and continuous in time. For a similar approach, regarding the temporal part of the discretization, see the recent contribution [12], where a *h*-version hybrid DG method in space, combined with a global continuous Galerkin approach in time is presented for the acoustic wave equation. However, we obtain a method, which allows for local *hp*-refinement in space *and* time, is energy-conserving and unconditionally stable. In section 2 the space-time finite element method for the time-dependent Maxwell equations

$$\begin{aligned}
\varepsilon \mathbf{E}_t - \nabla \times \mathbf{H} &= \mathbf{J} && \text{in } \Omega \times (0, T] \\
\mu \mathbf{H}_t + \nabla \times \mathbf{E} &= 0 && \text{in } \Omega \times (0, T] \\
\mathbf{n} \times \mathbf{E} &= \mathbf{n} \times \mathbf{g} && \text{on } \partial\Omega \times (0, T] \\
\mathbf{E} &= \mathbf{E}_0, \quad \mathbf{H} = \mathbf{H}_0 && \text{in } \Omega, \quad t = 0
\end{aligned} \tag{1}$$

is described, where  $\varepsilon(\mathbf{x}), \mu(\mathbf{x}) : \Omega \rightarrow \mathbb{R}$  denote the electric permittivity and magnetic permeability, respectively. In sections 3 and 4 we discuss the stability and energy conservation property of the method. In section 5 we present a matrix-free implementation of the space-time residual. It can be efficiently evaluated within an iterative solution procedure, such that the method computationally behaves similarly to an explicit method. Section 6 is devoted to numerical experiments, including fully space-time *hp*-adaptive simulations.

## 2. Description of the method

### 2.1. Function spaces

We will denote vector valued functions spaces with bold letters, e.g.  $\mathbf{L}_2(D) := [L_2(D)]^3$ . We introduce the spaces

$$\begin{aligned}
\mathbf{H}(\text{curl}, \Omega) &:= \{\mathbf{v} \in \mathbf{L}_2(\Omega) : \nabla \times \mathbf{v} \in \mathbf{L}_2(\Omega)\}, \\
\mathbf{H}_0(\text{curl}, \Omega) &:= \{\mathbf{v} \in \mathbf{L}_2(\Omega) : \nabla \times \mathbf{v} \in \mathbf{L}_2(\Omega), \mathbf{n} \times \mathbf{v} = 0 \text{ on } \partial\Omega\}.
\end{aligned}$$

For  $\mathbf{J} = 0, \mathbf{g} = 0$  the Maxwell system admits a unique solution  $\mathbf{U} = \{\mathbf{E}, \mathbf{H}\}$  in (see e.g. [13]):

$$\mathbf{V} := C^0([0, T], \mathbf{H}_0(\text{curl}, \Omega)) \cap C^1([0, T], \mathbf{L}_2(\Omega)) \times C^0([0, T], \mathbf{H}(\text{curl}, \Omega)) \cap C^1([0, T], \mathbf{L}_2(\Omega)).$$

### 2.2. Partitioning of the space-time domain

For the derivation of the method, we only consider spatial meshes consisting of hexahedra. Nevertheless, most of the presented work is applicable to tetrahedral meshes, as well.

We divide the time axis in intervals  $\mathcal{I}_n = (t_{n-1}, t_n]$ , and thus obtain a partitioning of the space-time cylinder  $\mathcal{I} \times \Omega$  in time slabs  $\mathcal{I}_n \times \Omega$ . For each time slab, the spatial domain  $\Omega$  is partitioned into non-overlapping (hexahedral) elements  $K$  resulting in a triangulation  $\mathcal{T}_n(\Omega)$ . We require that  $\mathcal{T}_n(\Omega)$  can be obtained by refinement of a coarse triangulation  $\overline{\mathcal{T}}(\Omega)$ . The obtained macro-elements are further bisected in temporal direction  $\mathcal{I}_n \times K = \bigcup_{k=1}^{N_K} I_k^K \times K$ , such that we obtain a partition of the time slab  $\mathcal{I}_n \times \Omega$  in space-time elements  $I_k^K \times K \in \mathcal{S}_n(\mathcal{I}_n \times \Omega)$ . Here  $\mathcal{S}_n(\mathcal{I}_n \times \Omega)$  denotes the resulting triangulation of the time slab.

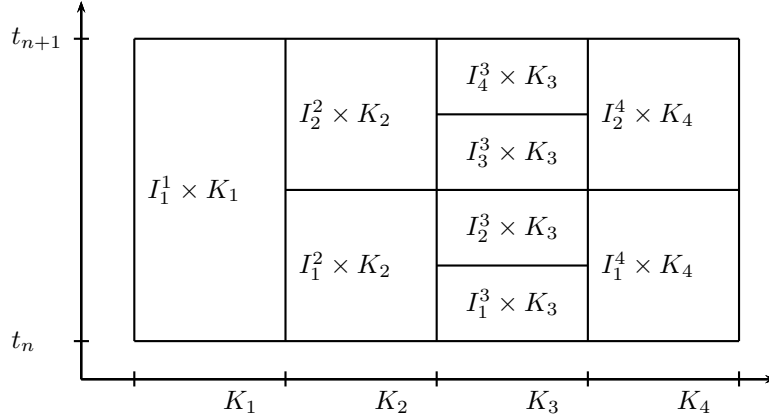


Figure 1: Space-time partitioning of a time-slab

### 2.3. Discrete spaces

Let  $F_K$  denote the mapping from the unit cube  $\hat{K} = [0, 1]^3$  with axes  $\hat{x}, \hat{y}, \hat{z}$  to the physical element  $K = F_K(\hat{K})$ . Furthermore by  $DF_K$  we denote the jacobian matrix of  $F_K$ . The electric and magnetic fields are transformed with the covariant transformation  $\mathbf{v}(x, t) = DF_K^{-T} \hat{\mathbf{v}}(\hat{x}, t) oF_K^{-1}$ , as proposed in [5]. By  $P_{p_t}(I)$  we denote polynomials of degree  $p_t$  on interval  $I$  and by  $Q_{p_x, p_y, p_z}(\hat{K})$

tensor product polynomials of degrees  $p_x, p_y$  and  $p_z$  in the  $\hat{x}, \hat{y}, \hat{z}$  directions. Now we can introduce the following local discrete spaces

$$V_{h,\hat{K}}^k := P_{p_t}(I_k^K) \otimes \left[ Q_{p_x,p_y,p_z}(\hat{K}) \right]^3 \quad (2)$$

$$W_{h,\hat{K}}^k := P_{p_t-1}(I_k^K) \otimes \left[ Q_{p_x,p_y,p_z}(\hat{K}) \right]^3. \quad (3)$$

$\mathbf{p}_k^K = (p_t, p_x, p_y, p_z)$  denotes the local polynomial degree vector assigned to the space-time elements  $I_k^K \times \hat{K}, k = 1, \dots, N_K$ . Note that the spatial part of the polynomial spaces in (2) is identical for all elements  $I_k^K \times \hat{K}$  in one macro-element  $\mathcal{I}_n \times \hat{K}$ . Thus we obtain, for each macro-element, tensor-product polynomial test- and trial-spaces consisting of a piecewise polynomial temporal trial- and test spaces  $S_K(\mathcal{I}_n)$  and  $T_K(\mathcal{I}_n)$  and the spatial part  $Q_{p_x,p_y,p_z}(\hat{K})$ .

$$\begin{aligned} V_{h,\hat{K}} &:= S_K(\mathcal{I}_n) \otimes \left[ Q_{p_x,p_y,p_z}(\hat{K}) \right]^3, & S_K(\mathcal{I}_n) &:= \{u(t) \in H^1(\mathcal{I}_n) : u|_{I_k^K} \in P_{p_t}(I_k^K)\} \\ W_{h,\hat{K}} &:= T_K(\mathcal{I}_n) \otimes \left[ Q_{p_x,p_y,p_z}(\hat{K}) \right]^3, & T_K(\mathcal{I}_n) &:= \{u(t) \in L_2(\mathcal{I}_n) : u|_{I_k^K} \in P_{p_t-1}(I_k^K)\}. \end{aligned} \quad (4)$$

We collect the local polynomial degree vectors for all elements in a global vector  $\mathbf{p}$ .

Now we can define the global spaces for one time-slab

$$V_h(\mathcal{I}_n \times \Omega; \mathbf{p}) := \{\mathbf{v}(t, \mathbf{x}) \in H^1(\mathcal{I}_n; L_2(\Omega)) : DF^T \mathbf{v}|_K \circ F \in V_{h,\hat{K}}\}, \quad (5)$$

and

$$W_h(\mathcal{I}_n \times \Omega; \mathbf{p}) := \{\mathbf{v}(t, \mathbf{x}) \in L_2(\mathcal{I}_n; L_2(\Omega)) : DF^T \mathbf{v}|_K \circ F \in W_{h,\hat{K}}\}. \quad (6)$$

While both spaces are spatially discontinuous, the functions in  $V_h$  and  $W_h$  have different continuity properties in temporal direction: functions in  $V_h$  are time-continuous within each time slab whereas functions in  $W_h$  are allowed to be discontinuous at the interfaces in time direction. The situation is depicted for an example with three space-time elements in Fig. 2.

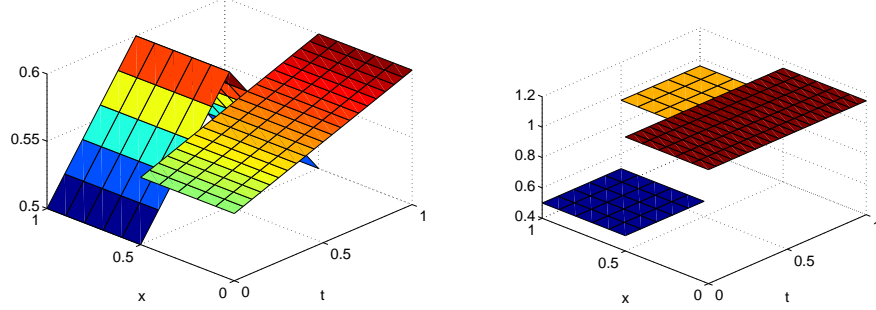


Figure 2: Left: function belonging to trial space  $V_h$ , right: function from the corresponding test space  $W_h$

#### 2.4. Faces and trace operators

By  $\mathcal{F}$  we denote the set of all faces in the spatial triangulation  $\mathcal{T}(\Omega)$ , by  $\mathcal{F}_0$  the set of all interior faces  $f := \partial K^1 \cap \partial K^2 : K^1, K^2 \in \mathcal{T}(\Omega)$  and by  $\mathcal{F}_b$  the set of all boundary faces  $f := \partial K \cap \partial \Omega : K \in \mathcal{T}(\Omega)$ .

We define on interior faces  $f \in \mathcal{F}_0$  the average and tangential jump operators as  $\{\mathbf{v}\} := (\mathbf{v}^1 + \mathbf{v}^2)/2$  and  $[[\mathbf{v}]]_T := \mathbf{n}^1 \times \mathbf{v}^1 + \mathbf{n}^2 \times \mathbf{v}^2$  respectively. Here  $\mathbf{v}^1$  and  $\mathbf{v}^2$  denote the traces of  $\mathbf{v}$  on  $f$  taken from within element  $K^1$  and  $K^2$  with unit normals  $\mathbf{n}^1$  and  $\mathbf{n}^2$ . For a boundary face  $f \in \mathcal{F}_b$  we define averages and jumps as  $\{\mathbf{v}\} := \mathbf{v}$  and  $[[\mathbf{v}]]_T := \mathbf{n} \times \mathbf{v}$ .

In the following section we consider the discretization of a single time-slab  $\mathcal{I}_n \times \Omega$ .

#### 2.5. Weak formulation

Multiplying (1) by smooth test functions  $\mathbf{v}, \mathbf{w}$ , integrating over a macroelement  $\mathcal{I}_n \times K$  and performing integration by parts of the terms involving the curl operator with respect to the spatial variables yields:

$$\begin{aligned}
& \int_{\mathcal{I}_n} \int_K \varepsilon \partial_t \mathbf{E} \cdot \mathbf{v} \, dx \, dt - \int_{\mathcal{I}_n} \int_K \mathbf{H} \cdot \nabla \times \mathbf{v} \, dx \, dt \\
& - \int_{\mathcal{I}_n} \int_{\partial K} \mathbf{n} \times \mathbf{H}^* \cdot \mathbf{v} \, dS \, dt = \int_{\mathcal{I}_n} \int_K \mathbf{J} \cdot \mathbf{v} \, dx \, dt \\
& \int_{\mathcal{I}_n} \int_K \mu \partial_t \mathbf{H} \cdot \mathbf{w} \, dx \, dt + \int_{\mathcal{I}_n} \int_K \nabla \times \mathbf{E} \cdot \mathbf{w} \, dx \, dt \\
& + \int_{\mathcal{I}_n} \int_{\partial K} \mathbf{n} \times (\mathbf{E}^* - \mathbf{E}) \cdot \mathbf{w} \, dS \, dt = 0. \tag{7}
\end{aligned}$$

Then by replacing  $\mathbf{U}_h := \{\mathbf{E}, \mathbf{H}\} \in \mathbf{V}$  by the discrete fields  $\mathbf{E}_h, \mathbf{H}_h \in V_h$ , summing over all  $\mathcal{I}_n \times K$  and choosing centered fluxes

$$\mathbf{n} \times \mathbf{E}^* = \mathbf{n} \times \{\mathbf{E}_h\} \, f \in \mathcal{F}_0, \quad \mathbf{n} \times \mathbf{E}^* = \mathbf{n} \times \mathbf{g} \, f \in \mathcal{F}_D, \quad \mathbf{n} \times \mathbf{H}^* = \mathbf{n} \times \{\mathbf{H}_h\}, \, f \in \mathcal{F}$$

one obtains

$$\begin{aligned}
C_h(\mathbf{U}_h, \mathbf{V}) &= L(\mathbf{V}) \\
C_h(\mathbf{U}_h, \mathbf{V}) &:= \int_{\mathcal{I}_n} \int_{\Omega} \varepsilon \partial_t \mathbf{E}_h \cdot \mathbf{v} \, dx \, dt + \int_{\mathcal{I}_n} \int_{\Omega} \mu \partial_t \mathbf{H}_h \cdot \mathbf{w} \, dx \, dt + \\
&\quad - \int_{\mathcal{I}_n} \int_{\Omega} \mathbf{H}_h \cdot \nabla_h \times \mathbf{v} \, dx \, dt + \int_{\mathcal{I}_n} \int_{\Omega} \nabla_h \times \mathbf{E}_h \cdot \mathbf{w} \, dx \, dt \\
&\quad + \int_{\mathcal{I}_n} \int_{\mathcal{F}_0 \cup \mathcal{F}_b} \{\mathbf{H}_h\} \cdot \llbracket \mathbf{v} \rrbracket_T \, dS \, dt - \int_{\mathcal{I}_n} \int_{\mathcal{F}_0 \cup \mathcal{F}_b} \llbracket \mathbf{E}_h \rrbracket_T \cdot \{\mathbf{w}\} \, dS \, dt \quad (8) \\
L(\mathbf{V}) &:= \ell_E(\mathbf{v}) + \ell_H(\mathbf{w}) \\
\ell_E(\mathbf{v}) &= \int_{\mathcal{I}_n} \int_{\Omega} \mathbf{J} \cdot \mathbf{v} \, dx \, dt, \quad \ell_H(\mathbf{w}) = - \int_{\mathcal{I}_n} \int_{\mathcal{F}_b} \mathbf{n} \times \mathbf{g} \cdot \mathbf{w} \, dS \, dt. \quad (9)
\end{aligned}$$

### 3. Stability - discretizations with global $hp$ -refinement in time

In this section we provide stability results in the  $L_2(\Omega)$ - and  $L_2(\mathcal{I}; \mathbf{L}_2(\Omega))$ -norms. In order to obtain the stability bounds, we apply techniques similar to those presented in [12]. We restrict the analysis to discretizations, where  $T_K(\mathcal{I}_n)$  does not depend on the spatial element  $K$ , i.e. no local refinement with respect to time is present.

We consider the problem

$$\begin{aligned}
&\text{Find } \mathbf{U}_h \in V_h \times V_h \quad \text{such that} \\
&C_h(\mathbf{U}_h, \mathbf{V}) = L(\mathbf{V}) \quad \forall \mathbf{V} \in W_h \times W_h. \quad (10)
\end{aligned}$$

The general case, including local refinement in time, will be treated in the next section.

#### 3.1. Stability: $L_2(\Omega)$ – Norm

Denoting the discrete electromagnetic energy by

$$\mathcal{E}(t) = \frac{1}{2} \int_{\Omega} (\varepsilon \mathbf{E}_h \cdot \mathbf{E}_h + \mu \mathbf{H}_h \cdot \mathbf{H}_h) \, dx, \quad (11)$$

we demonstrate stability of the method by showing, that the energy is constant up to a contribution of the source terms. This result is a discrete version of Poyntings theorem (see e.g. [14]), which holds for the continuous Maxwell system.

**Theorem 3.1.** *Provided, the temporal polynomial degree  $p_t$  is uniform for all  $\mathcal{I}_n \times K$  and the material parameters  $\varepsilon, \mu$  are element-wise constant*

$$\mathcal{E}(t_{n+1}) - \mathcal{E}(t_n) = \int_{\mathcal{I}_n} \int_{\Omega} \mathbf{J} \cdot \pi \mathbf{E}_h \, dx \, dt - \int_{\mathcal{I}_n} \int_{\mathcal{F}_b} \mathbf{n} \times \mathbf{g} \cdot \pi \mathbf{H}_h \, dS \, dt. \quad (12)$$

*Proof.* We denote by  $\pi\mathbf{E}_h, \pi\mathbf{H}_h$  the  $L_2$ -orthogonal projections of the discrete solution onto the test space  $W_h$ . Please note, that this projection reduces to a projection with respect to time only, since the spatial parts of the tensor-product trial- and testspaces coincide.

Choosing  $\mathbf{v} = \pi\mathbf{E}_h, \mathbf{w} = \pi\mathbf{H}_h$  in (10) yields

$$\begin{aligned}
& \int_{\mathcal{I}_n} \int_{\Omega} \varepsilon \partial_t \mathbf{E}_h \cdot \pi \mathbf{E}_h \, dx \, dt + \int_{\mathcal{I}_n} \int_{\Omega} \mu \partial_t \mathbf{H}_h \cdot \pi \mathbf{H}_h \, dx \, dt \\
& - \int_{\mathcal{I}_n} \int_{\Omega} \mathbf{H}_h \cdot \nabla_h \times \pi \mathbf{E}_h \, dx \, dt + \int_{\mathcal{I}_n} \int_{\Omega} \nabla_h \times \mathbf{E}_h \cdot \pi \mathbf{H}_h \, dx \, dt \\
& + \int_{\mathcal{I}_n} \int_{\mathcal{F}_0 \cup \mathcal{F}_b} \{\mathbf{H}_h\} \cdot \llbracket \pi \mathbf{E}_h \rrbracket_T \, dS \, dt - \int_{\mathcal{I}_n} \int_{\mathcal{F}_0 \cup \mathcal{F}_b} \llbracket \mathbf{E}_h \rrbracket_T \cdot \{\pi \mathbf{H}_h\} \, dS \, dt \\
& = \int_{\mathcal{I}_n} \int_{\Omega} \mathbf{J} \cdot \pi \mathbf{E}_h \, dx \, dt - \int_{\mathcal{I}_n} \int_{\mathcal{F}_b} \mathbf{n} \times \mathbf{g} \cdot \pi \mathbf{H}_h \, dS \, dt \tag{13}
\end{aligned}$$

Since  $\partial_t \mathbf{E}_h \in W_h$  and by using integration by parts, we obtain for the first term in (13)

$$\begin{aligned}
\int_{\mathcal{I}_n} \int_{\Omega} \varepsilon \partial_t \mathbf{E}_h \cdot \pi \mathbf{E}_h \, dx \, dt &= \int_{\mathcal{I}_n} \int_{\Omega} \varepsilon \partial_t \mathbf{E}_h \cdot \mathbf{E}_h \, dx \, dt \\
&= \frac{1}{2} \int_{\Omega} \varepsilon \mathbf{E}_h(t_{k+1}) \cdot \mathbf{E}_h(t_{k+1}) \, dx - \frac{1}{2} \int_{\Omega} \varepsilon \mathbf{E}_h(t_k) \cdot \mathbf{E}_h(t_k) \, dx.
\end{aligned}$$

Thus we obtain by treating the second term in (13) the same way

$$\int_{\mathcal{I}_n} \int_{\Omega} \varepsilon \partial_t \mathbf{E}_h \cdot \pi \mathbf{E}_h \, dx \, dt + \int_{\mathcal{I}_n} \int_{\Omega} \mu \partial_t \mathbf{H}_h \cdot \pi \mathbf{H}_h \, dx \, dt = \mathcal{E}(t_{n+1}) - \mathcal{E}(t_n). \tag{14}$$

The third term yields

$$- \int_{\mathcal{I}_n} \int_{\Omega} \mathbf{H}_h \cdot \nabla_h \times \pi \mathbf{E}_h \, dx \, dt = - \int_{\mathcal{I}_n} \int_{\Omega} \pi \mathbf{H}_h \cdot \nabla_h \times \mathbf{E}_h \, dx \, dt$$

where we have used that  $\pi$  is an orthogonal projection and thus self-adjoint. Thus, the sum of the third and fourth terms is zero.

Now, consider the mesh-dependent terms associated with an interior face  $f =$

$\partial K^1 \cap \partial K^2 \in \mathcal{F}_0$ . We have by a straightforward calculation

$$\begin{aligned}
& + \int_{\mathcal{I}_n} \int_f \{\mathbf{H}_h\} \cdot \llbracket \pi \mathbf{E}_h \rrbracket_T \, dS \, dt - \int_{\mathcal{I}_n} \int_f \llbracket \mathbf{E}_h \rrbracket_T \cdot \{\pi \mathbf{H}_h\} \, dS \, dt \\
& = \frac{1}{2} \int_{\mathcal{I}_n} \int_f \mathbf{H}_h^1 \cdot \mathbf{n}^1 \times \pi^1 \mathbf{E}^1 \, dS \, dt + \frac{1}{2} \int_{\mathcal{I}_n} \int_f \mathbf{H}_h^2 \cdot \mathbf{n}^1 \times \pi^1 \mathbf{E}_h^1 \, dS \, dt \\
& + \frac{1}{2} \int_{\mathcal{I}_n} \int_f \mathbf{H}_h^1 \cdot \mathbf{n}^2 \times \pi^2 \mathbf{E}^2 \, dS \, dt + \frac{1}{2} \int_{\mathcal{I}_n} \int_f \mathbf{H}_h^2 \cdot \mathbf{n}^2 \times \pi^2 \mathbf{E}^2 \, dS \, dt \\
& - \frac{1}{2} \int_{\mathcal{I}_n} \int_f \pi^1 \mathbf{H}^1 \cdot \mathbf{n}^1 \times \mathbf{E}_h^1 \, dS \, dt - \frac{1}{2} \int_{\mathcal{I}_n} \int_f \pi^1 \mathbf{H}^1 \cdot \mathbf{n}^2 \times \mathbf{E}_h^2 \, dS \, dt \\
& - \frac{1}{2} \int_{\mathcal{I}_n} \int_f \pi^2 \mathbf{H}^2 \cdot \mathbf{n}^1 \times \mathbf{E}_h^1 \, dS \, dt - \frac{1}{2} \int_{\mathcal{I}_n} \int_f \pi^2 \mathbf{H}^2 \cdot \mathbf{n}^2 \times \mathbf{E}_h^2 \, dS \, dt \quad (15) \\
& = T_1 + T_2 + T_3 + T_4 + T_5 + T_6 + T_7 + T_8,
\end{aligned}$$

where  $\pi^1$  and  $\pi^2$  denote the restrictions of the projection  $\pi$  to local spaces  $W_{h,K^1}$  and  $W_{h,K^2}$  from (4).

First, we inspect the terms, which do not couple to neighboring elements, for example  $T_1$  and  $T_5$  (15). Again, by the symmetry of  $\pi^1$ , we have for the first term

$$T_1 = \frac{1}{2} \int_{\mathcal{I}_n} \int_f \mathbf{H}_h^1 \cdot \mathbf{n}^1 \times \pi^1 \mathbf{E}^1 \, dS \, dt = \frac{1}{2} \int_{\mathcal{I}_n} \int_f \pi^1 \mathbf{H}^1 \cdot \mathbf{n}^1 \times \mathbf{E}_h^1 \, dS \, dt = -T_5,$$

such that  $T_1 + T_5 = 0$ . Analogously we obtain  $T_4 + T_8 = 0$ .

For the terms involving neighbor-coupling there holds, for example,

$$\begin{aligned}
T_2 & = \frac{1}{2} \int_{\mathcal{I}_n} \int_f \mathbf{H}_h^2 \cdot \mathbf{n}^1 \times \pi^1 \mathbf{E}^1 \, dS \, dt = \frac{1}{2} \int_{\mathcal{I}_n} \int_f \pi^1 \mathbf{H}_h^2 \cdot \mathbf{n}^1 \times \mathbf{E}_h^1 \, dS \, dt \\
& = \frac{1}{2} \int_{\mathcal{I}_n} \int_f \pi^2 \mathbf{H}_h^2 \cdot \mathbf{n}^1 \times \mathbf{E}_h^1 \, dS \, dt = -T_7,
\end{aligned}$$

thus, we obtain  $T_2 + T_7 = 0$  and similarly  $T_3 + T_6 = 0$ .

Note, that this holds only due to  $\pi^1 \mathbf{H}_h^2 = \pi^2 \mathbf{H}_h^2$ , which is fulfilled since the temporal parts  $T_{K^1}(\mathcal{I}_n)$  and  $T_{K^2}(\mathcal{I}_n)$  of the local test spaces  $W_{h,K^1}$  and  $W_{h,K^2}$  are identical for all elements, which in turn is achieved by the restriction to discretizations without local refinement in time.

Noting that terms associated with a boundary face can be treated exactly the same way as the non-coupling terms, yields the desired result.  $\square$

### 3.2. Stability $L_2(\mathcal{I}; L_2(\Omega))$ -Norm

For the special case of no local refinement in time we can also show the stability in the space-time  $L_2$ -norm  $\|\cdot\|_{L_2(\mathcal{I}; L_2(\Omega))}$ . First we recall the recurrence relations for the Legendre-polynomials  $L_i(\xi)$

$$\begin{aligned}
& (i+1)L_{i+1}(\xi) = (2i+1)\xi L_i(\xi) - iL_{i-1}(\xi) \\
& L'_i(\xi) = 2L_{i-1}(\xi)/\|L_{i-1}\|_{L_2([-1,1])}^2 + 2L_{i-3}(\xi)/\|L_{i-3}\|_{L_2([-1,1])}^2 + \dots \\
& \xi L'_{i+1} = (i+1)L_{i+1}(\xi) + iL_{i-1}(\xi) + (i-1)L_{i-1}(\xi) + (i-2)L_{i-3}(\xi) \dots \quad (16)
\end{aligned}$$



**Lemma 3.1.** *For element wise constant  $\varepsilon, \mu$  there holds*

$$\begin{aligned} \frac{1}{2\Delta t} \|\varepsilon^{\frac{1}{2}} \mathbf{E}_h\|_{L_2(\mathcal{I}_n; \mathbf{L}_2(\Omega))}^2 + \frac{1}{2\Delta t} \|\mu^{\frac{1}{2}} \mathbf{H}_h\|_{L_2(\mathcal{I}_n; \mathbf{L}_2(\Omega))}^2 &\leq \int_{\mathcal{I}_n} \int_{\Omega} \varepsilon \partial_t \mathbf{E}_h \cdot \pi(\tau(t) \pi \mathbf{E}_h) \, dx \, dt \\ &+ \int_{\mathcal{I}_n} \int_{\Omega} \mu \partial_t \mathbf{H}_h \cdot \pi(\tau(t) \pi \mathbf{H}_h) \, dx \, dt + \mathcal{E}(t_k), \quad \tau(t) = \frac{(t_{k+1} - t)}{\Delta t} \end{aligned}$$

*Proof.* We have by integration by parts with respect to the temporal variable

$$\int_{\mathcal{I}_n} \int_K \varepsilon \partial_t \mathbf{E}_h \cdot \pi(\tau(t) \mathbf{E}_h) \, dx \, dt = \frac{1}{2\Delta t} \|\varepsilon^{\frac{1}{2}} \mathbf{E}_h\|_{L_2(\mathcal{I}_n; \mathbf{L}_2(\Omega))}^2 - \frac{1}{2} \|\varepsilon^{\frac{1}{2}} \mathbf{E}_h(t_k)\|_K^2$$

using that  $\pi$  is an orthogonal projection and  $\partial_t \mathbf{E}_h \in W_h$  we can rewrite

$$\begin{aligned} \int_{\mathcal{I}_n} \int_K \varepsilon \partial_t \mathbf{E}_h \cdot \pi(\tau(t) \mathbf{E}_h) \, dx \, dt &= \int_{\mathcal{I}_n} \int_K \varepsilon \partial_t \mathbf{E}_h \cdot \tau(t) (\mathbf{E}_h - \pi \mathbf{E}_h) \, dx \, dt \\ &+ \int_{\mathcal{I}_n} \int_K \varepsilon \partial_t \mathbf{E}_h \cdot \tau(t) \pi \mathbf{E}_h \, dx \, dt. \quad (17) \end{aligned}$$

We will now show that the first term on the right-hand side of (17) is non-positive. Due to the space-time tensor product construction of the local finite element space, we can expand the discrete solution and the projection error as

$$\begin{aligned} \mathbf{E}_h &= \sum_{i=0}^{p_t} \sum_{k=1}^{N_s} L_i(\xi) \varphi_k(x, y, z) e_{ik} \\ \mathbf{E}_h - \pi \mathbf{E}_h &= \sum_{k=1}^{N_s} L_{p_t}(\xi) \varphi_k(x, y, z) e_{p_t k} \end{aligned} \quad (18)$$

with  $\xi = 2(t - t_k)/\Delta t - 1$  and  $N_s = 3(p_x + 1)(p_y + 1)(p_z + 1)$ . Using once more the projection property, inserting the expansions (18) we obtain

$$\begin{aligned} \int_{I_k^K} \int_K \varepsilon \partial_t \mathbf{E}_h \cdot \tau(t) (\mathbf{E}_h - \pi \mathbf{E}_h) \, dx \, dt &= -\frac{\varepsilon}{\Delta t} \int_{I_k^K} \int_K \partial_t \mathbf{E}_h \cdot t (\mathbf{E}_h - \pi \mathbf{E}_h) \, dx \, dt \\ &= -\frac{\varepsilon}{\Delta t} \sum_{i=1}^{p_t} \sum_{j=1}^{N_s} \sum_{l=1}^{N_s} \int_{-1}^1 (t_k + \Delta t(1 + \xi)/2) L'_i(\xi) L_{p_t}(\xi) \, d\xi \\ &\times \int_K \varphi_j(x, y, z) \cdot \varphi_l(x, y, z) \, dx e_{ij} e_{p_t l} \\ &= -\frac{\varepsilon}{\Delta t} \sum_{i=1}^{p_t} \int_{-1}^1 \frac{\Delta t}{2} \xi L'_i(\xi) L_{p_t+1}(\xi) \, d\xi \sum_{j=1}^{N_s} \sum_{l=1}^{N_s} \int_K \varphi_j(x, y, z) \cdot \varphi_l(x, y, z) \, dx e_{ij} e_{p_t l}. \end{aligned}$$

In the last step we have used the recurrence relation for the derivatives of Legendre polynomials. Finally, using the third recurrence relation in (16), we obtain

by the orthogonality of the Legendre polynomials

$$\begin{aligned}
& \int_{I_k^K} \int_K \varepsilon \partial_t \mathbf{E}_h \cdot \tau(t) (\mathbf{E}_h - \pi \mathbf{E}_h) \, dx \, dt \\
&= -(\varepsilon/2) \int_{-1}^1 L_{p_t}(\xi)^2 \, d\xi \sum_{j=1}^{N_s} \sum_{l=1}^{N_s} \int_K \boldsymbol{\varphi}_j(x, y, z) \cdot \boldsymbol{\varphi}_l(x, y, z) \, dx \, e_{p_t+1j} e_{p_t+1l} \leq 0
\end{aligned}$$

□

Denoting the dual norm on the discrete test space by

$$\|\ell\|_{W'_h} := \sup_{\mathbf{v} \in W_h} \frac{|\ell(\mathbf{v})|}{\|\mathbf{v}\|_{L_2(\mathcal{I}_n; \mathbf{L}_2(\Omega))}},$$

we can show

**Lemma 3.2.** *Provided, the temporal polynomial degree  $p_t$  is constant and no local  $h$ -refinement with respect to time is present in the discretization, for elementwise constant  $\varepsilon \geq \underline{\varepsilon} > 0$  and  $\mu \geq \underline{\mu} > 0$  there holds*

$$\|\varepsilon^{\frac{1}{2}} \mathbf{E}_h\|_{L_2(\mathcal{I}_n; \mathbf{L}_2(\Omega))}^2 + \|\mu^{\frac{1}{2}} \mathbf{H}_h\|_{L_2(\mathcal{I}_n; \mathbf{L}_2(\Omega))}^2 \leq 4\Delta t^2 \left( \underline{\varepsilon}^{-1} \|\ell_E\|_{W'_h}^2 + \underline{\mu}^{-1} \|\ell_H\|_{W'_h}^2 \right) + 4\Delta t \mathcal{E}(t_k) \tag{19}$$

*Proof.* Choosing  $\mathbf{v} = \pi(\tau(t)\pi\mathbf{E}_h)$ ,  $\mathbf{w} = \pi(\tau(t)\pi\mathbf{H}_h)$  in (10) yields

$$\begin{aligned}
& \int_{\mathcal{I}_n} \int_{\Omega} \varepsilon \partial_t \mathbf{E}_h \cdot \pi(\tau(t)\pi\mathbf{E}_h) \, dx \, dt + \int_{\mathcal{I}_n} \int_{\Omega} \mu \partial_t \mathbf{H}_h \cdot \pi(\tau(t)\pi\mathbf{H}_h) \, dx \, dt \\
& - \int_{\mathcal{I}_n} \int_{\Omega} \mathbf{H}_h \cdot \nabla_h \times \pi(\tau(t)\pi\mathbf{E}_h) \, dx \, dt + \int_{\mathcal{I}_n} \int_{\Omega} \nabla_h \times \mathbf{E}_h \cdot \pi(\tau(t)\pi\mathbf{H}_h) \, dx \, dt \\
& + \int_{\mathcal{I}_n} \int_{\mathcal{F}_0 \cup \mathcal{F}_b} \{\mathbf{H}_h\} \cdot \llbracket \pi(\tau(t)\pi\mathbf{E}_h) \rrbracket_T \, dS \, dt - \int_{\mathcal{I}_n} \int_{\mathcal{F}_0 \cup \mathcal{F}_b} \llbracket \mathbf{E}_h \rrbracket_T \cdot \{\pi(\tau(t)\pi\mathbf{H}_h)\} \, dS \, dt \\
& = \ell_E(\pi(\tau(t)\pi\mathbf{E}_h)) + \ell_H(\pi(\tau(t)\pi\mathbf{H}_h)). \tag{20}
\end{aligned}$$

Following the line of arguments of the proof of Theorem 3.1, all terms, except the first two terms on the left-hand side of (20) vanish.

Applying lemma 3.1, the Cauchy-Schwarz inequality, the arithmetic-geometric-

mean inequality yields

$$\begin{aligned}
& \frac{1}{2\Delta t} \left( \|\varepsilon^{\frac{1}{2}} \mathbf{E}_h\|_{L_2(\mathcal{I}_n; \mathbf{L}_2(\Omega))}^2 + \|\varepsilon^{\frac{1}{2}} \mathbf{H}_h\|_{L_2(\mathcal{I}_n; \mathbf{L}_2(\Omega))}^2 \right) \\
& \leq \ell_E(\pi(\tau(t)\pi \mathbf{E}_h)) + \ell_H(\pi(\tau(t)\pi \mathbf{H}_h)) + \mathcal{E}(t_k) \\
\leq & \|\ell_E\|_{W'_h} \|\pi(\tau(t)\pi \mathbf{E}_h)\|_{L_2(\mathcal{I}_n; \mathbf{L}_2(\Omega))} + \|\ell_H\|_{W'_h} \|\pi(\tau(t)\pi \mathbf{H}_h)\|_{L_2(\mathcal{I}_n; \mathbf{L}_2(\Omega))} + \mathcal{E}(t_k) \\
& \leq \Delta t \left( \underline{\varepsilon}^{-1} \|\ell_E\|_{W'_h}^2 + \underline{\mu}^{-1} \|\ell_H\|_{W'_h}^2 \right) + \mathcal{E}(t_k) \\
& + \frac{\underline{\varepsilon}}{4\Delta t} \|\pi(\tau(t)\pi \mathbf{E}_h)\|_{L_2(\mathcal{I}_n; \mathbf{L}_2(\Omega))}^2 + \frac{\underline{\mu}}{4\Delta t} \|\pi(\tau(t)\pi \mathbf{H}_h)\|_{L_2(\mathcal{I}_n; \mathbf{L}_2(\Omega))}^2 \\
& \leq \Delta t \left( \underline{\varepsilon}^{-1} \|\ell_E\|_{W'_h}^2 + \underline{\mu}^{-1} \|\ell_H\|_{W'_h}^2 \right) + \mathcal{E}(t_k) \\
& + \frac{1}{4\Delta t} \left( \|\varepsilon^{\frac{1}{2}} \pi(\tau(t)\pi \mathbf{E}_h)\|_{L_2(\mathcal{I}_n; \mathbf{L}_2(\Omega))}^2 + \|\mu^{\frac{1}{2}} \pi(\tau(t)\pi \mathbf{H}_h)\|_{L_2(\mathcal{I}_n; \mathbf{L}_2(\Omega))}^2 \right).
\end{aligned}$$

Since  $\|\pi\| \leq 1$  and  $1 \geq \tau(t) \geq 0$  on  $\mathcal{I}_n$ , we obtain the result.  $\square$

**Theorem 3.2.** *Provided the temporal polynomial degree  $p_t$  is constant and no local  $h$ -refinement with respect to time is present in the discretization there holds for elementwise constant  $\varepsilon \geq \underline{\varepsilon} > 0$  and  $\mu \geq \underline{\mu} > 0$*

$$\mathcal{E}(t_n) \leq 2\mathcal{E}(t_1) + 2 \sum_{n=1}^N \left( \left( \frac{2t_n}{\underline{\varepsilon}} + \frac{\Delta t^2}{2t_n \underline{\varepsilon}} \right) \|\ell_E^k\|_{W'_h}^2 + \left( \frac{2t_n}{\underline{\mu}} + \frac{\Delta t^2}{2t_n \underline{\mu}} \right) \|\ell_H^k\|_{W'_h}^2 \right) \quad (21)$$

*Proof.* The proof follows along the lines of [12] Corollary 1.

Denoting  $n_{max} = \arg \max_n \mathcal{E}(t_n)$ , we have by Theorem 3.1 and the Cauchy-Schwarz inequality, the arithmetic geometric mean inequality, (19)

$$\begin{aligned}
\max_n \mathcal{E}(t_n) & \leq \mathcal{E}(t_1) + \sum_{n=1}^{n_{max}} \left( \|\ell_E\|_{W'_h} \|\mathbf{E}_h\|_{L_2(\mathcal{I}_n; \mathbf{L}_2(\Omega))} + \|\ell_H\|_{W'_h} \|\mathbf{H}_h\|_{L_2(\mathcal{I}_n; \mathbf{L}_2(\Omega))} \right) \\
& \leq \mathcal{E}(t_1) + \sum_{n=1}^{n_{max}} \left( \frac{\delta}{\underline{\varepsilon}} \|\ell_E\|_{W'_h}^2 + \frac{\delta}{\underline{\mu}} \|\ell_H\|_{W'_h}^2 + \frac{\underline{\varepsilon}}{4\delta} \|\mathbf{E}_h\|_{L_2(\mathcal{I}_n; \mathbf{L}_2(\Omega))}^2 + \frac{\underline{\mu}}{4\delta} \|\mathbf{H}_h\|_{L_2(\mathcal{I}_n; \mathbf{L}_2(\Omega))}^2 \right) \\
& \leq \mathcal{E}(t_1) + \sum_{n=1}^{n_{max}} \left( \left( \frac{\delta}{\underline{\varepsilon}} + \frac{\Delta t^2}{\underline{\varepsilon} \delta} \right) \|\ell_E\|_{W'_h}^2 + \left( \frac{\delta}{\underline{\mu}} + \frac{\Delta t^2}{\underline{\mu} \delta} \right) \|\ell_H\|_{W'_h}^2 + \frac{\Delta t}{\delta} \mathcal{E}(t_n) \right).
\end{aligned}$$

Chosing  $\delta = 2t_{n_{max}}$  we have

$$\sum_{n=1}^{n_{max}} \frac{\Delta t}{2t_{n_{max}}} \mathcal{E}(t_n) \leq \frac{1}{2} \max_n \mathcal{E}(t_n),$$

and thus the estimate for  $\mathcal{E}(t_n)$ , which can be applied to the corresponding term in (19).  $\square$

#### 4. Stability - discretizations with local $hp$ -refinement in time

In this section we show, that stability in the  $L_2(\Omega)$ -norm can be obtained also for discretizations with local  $hp$ -refinement in time. This is achieved by adding a suitable stabilization term, which amounts to restoring anti-symmetry in the coupling flux terms.

##### 4.1. Stability: $L_2(\Omega)$ - Norm

For an interior space-time face  $\mathcal{I}_n \times f$ ,  $f \in \mathcal{F}_0$  shared by  $\mathcal{I}_n \times K^i$ ,  $i = 1, 2$ , we denote by  $\mathcal{P}_f : L_2(\mathcal{I}_n) \rightarrow \tilde{T}(\mathcal{I}_n)$  the  $L_2$ -orthogonal projection operator onto the largest common temporal testspace  $\tilde{T}(\mathcal{I}_n) := T_{K^1}(\mathcal{I}_n) \cap T_{K^2}(\mathcal{I})$ . Further we denote by  $\tilde{\pi}$  the projector whose restriction to  $\mathcal{I}_n \times f$  is  $\tilde{\pi}_f$ .

We add the stabilization form

$$\begin{aligned} S_h(\mathbf{U}_h, \mathbf{V}) := & \frac{1}{2} \left( \int_{\mathcal{I}_n} \int_{\mathcal{F}_0} \{\mathbf{H}_h\} \cdot \llbracket \tilde{\pi} \mathbf{v} - \mathbf{v} \rrbracket_T dS dt + \int_{\mathcal{I}_n} \int_{\mathcal{F}_0} \llbracket \mathbf{H}_h \rrbracket_T \cdot \{\tilde{\pi} \mathbf{v} - \mathbf{v}\} dS dt \right) \\ & - \frac{1}{2} \left( \int_{\mathcal{I}_n} \int_{\mathcal{F}_0} \{\mathbf{E}_h\} \cdot \llbracket \tilde{\pi} \mathbf{w} - \mathbf{w} \rrbracket_T dS dt + \int_{\mathcal{I}_n} \int_{\mathcal{F}_0} \llbracket \mathbf{E}_h \rrbracket_T \cdot \{\tilde{\pi} \mathbf{w} - \mathbf{w}\} dS dt \right). \end{aligned} \quad (22)$$

and obtain the stabilized discrete problem

$$\begin{aligned} & \text{Find } \mathbf{U}_h \in V_h \times V_h \\ & B_h(\mathbf{U}_h, \mathbf{V}) := C_h(\mathbf{U}_h, \mathbf{V}) + S_h(\mathbf{U}_h, \mathbf{V}) = L(\mathbf{V}) \quad \forall \mathbf{V} \in W_h \times W_h. \end{aligned} \quad (23)$$

Note, that in the case of globally in time refined discretization, as considered in the previous section, we obtain  $S_h(\mathbf{U}_h, \mathbf{V}) = 0$  and (23) reduces to (10).

Now we can generalize theorem 3.1 to discretizations with local  $hp$ -refinement in time:

**Theorem 4.1.** *For element-wise constant material parameters  $\varepsilon, \mu$*

$$\mathcal{E}(t_{n+1}) - \mathcal{E}(t_n) = \int_{\mathcal{I}_n} \int_{\Omega} \mathbf{J} \cdot \pi \mathbf{E}_h dx dt - \int_{\mathcal{I}_n} \int_{\mathcal{F}_b} \mathbf{n} \times \mathbf{g} \cdot \pi \mathbf{H}_h dS dt. \quad (24)$$

*Proof.* Regarding the treatment of the volume integrals and boundary faces, the proof is identical to the one of theorem 3.1. Thus, in the following we will only consider the mesh-dependent terms associated with interior faces  $f \in \mathcal{F}_0$ .

Again, we denote by  $\pi \mathbf{E}_h, \pi \mathbf{H}_h$  the  $L_2$ -projections of the discrete solution onto

the test space. Choosing  $\mathbf{v} = \pi \mathbf{E}_h$ ,  $\mathbf{w} = \pi \mathbf{H}_h$  in (23) yields

$$\begin{aligned}
& \int_{\mathcal{I}_n} \int_{\Omega} \varepsilon \partial_t \mathbf{E}_h \cdot \pi \mathbf{E}_h \, dx \, dt + \int_{\mathcal{I}_n} \int_{\Omega} \mu \partial_t \mathbf{H}_h \cdot \pi \mathbf{H}_h \, dx \, dt \\
& - \int_{\mathcal{I}_n} \int_{\Omega} \mathbf{H}_h \cdot \nabla_h \times \pi \mathbf{E}_h \, dx \, dt + \int_{\mathcal{I}_n} \int_{\Omega} \nabla_h \times \mathbf{E}_h \cdot \pi \mathbf{H}_h \, dx \, dt \\
& + \int_{\mathcal{I}_n} \int_{\mathcal{F}_0 \cup \mathcal{F}_b} \{\mathbf{H}_h\} \cdot \llbracket \pi \mathbf{E}_h \rrbracket_T \, dS \, dt - \int_{\mathcal{I}_n} \int_{\mathcal{F}_0 \cup \mathcal{F}_b} \llbracket \mathbf{E}_h \rrbracket_T \cdot \{\pi \mathbf{H}_h\} \, dS \, dt \\
& + \frac{1}{2} \left( \int_{\mathcal{I}_n} \int_{\mathcal{F}_0} \{\mathbf{H}_h\} \cdot \llbracket \tilde{\pi} \pi \mathbf{E}_h - \pi \mathbf{E}_h \rrbracket_T \, dS \, dt + \int_{\mathcal{I}_n} \int_{\mathcal{F}_0} \llbracket \mathbf{H}_h \rrbracket_T \cdot \{\tilde{\pi} \pi \mathbf{E}_h - \pi \mathbf{E}_h\} \, dS \, dt \right) \\
& - \frac{1}{2} \left( \int_{\mathcal{I}_n} \int_{\mathcal{F}_0} \{\mathbf{E}_h\} \cdot \llbracket \tilde{\pi} \pi \mathbf{H}_h - \pi \mathbf{H}_h \rrbracket_T \, dS \, dt + \int_{\mathcal{I}_n} \int_{\mathcal{F}_0} \llbracket \mathbf{E}_h \rrbracket_T \cdot \{\tilde{\pi} \pi \mathbf{H}_h - \pi \mathbf{H}_h\} \, dS \, dt \right) \\
& = \int_{\mathcal{I}_n} \int_{\Omega} \mathbf{J} \cdot \pi \mathbf{E}_h \, dx \, dt - \int_{\mathcal{I}_n} \int_{\mathcal{F}_b} \mathbf{n} \times \mathbf{g} \cdot \pi \mathbf{H}_h \, dS \, dt \tag{25}
\end{aligned}$$

Algebraic manipulations lead to

$$\begin{aligned}
& \int_{\mathcal{I}_n} \int_f \{\mathbf{H}_h\} \cdot \llbracket \pi \mathbf{E}_h \rrbracket_T \, dS \, dt - \int_{\mathcal{I}_n} \int_f \llbracket \mathbf{E}_h \rrbracket_T \cdot \{\pi \mathbf{H}_h\} \, dS \, dt \\
& + \frac{1}{2} \left( \int_{\mathcal{I}_n} \int_f \{\mathbf{H}_h\} \cdot \llbracket \tilde{\pi}_f \pi \mathbf{E}_h - \pi \mathbf{E}_h \rrbracket_T \, dS \, dt + \int_{\mathcal{I}_n} \int_f \llbracket \mathbf{H}_h \rrbracket_T \cdot \{\tilde{\pi}_f \pi \mathbf{E}_h - \pi \mathbf{E}_h\} \, dS \, dt \right) \\
& - \frac{1}{2} \left( \int_{\mathcal{I}_n} \int_f \{\mathbf{E}_h\} \cdot \llbracket \tilde{\pi}_f \pi \mathbf{H}_h - \pi \mathbf{H}_h \rrbracket_T \, dS \, dt + \int_{\mathcal{I}_n} \int_f \llbracket \mathbf{E}_h \rrbracket_T \cdot \{\tilde{\pi}_f \pi \mathbf{H}_h - \pi \mathbf{H}_h\} \, dS \, dt \right) \\
& = \frac{1}{2} \int_{\mathcal{I}_n} \int_f \mathbf{H}_h^1 \cdot \mathbf{n}^1 \times \pi^1 \mathbf{E}_h^1 \, dS \, dt + \frac{1}{2} \int_{\mathcal{I}_n} \int_f \mathbf{H}_h^2 \cdot \mathbf{n}^1 \times \tilde{\pi}_f \pi^1 \mathbf{E}_h^1 \, dS \, dt \\
& + \frac{1}{2} \int_{\mathcal{I}_n} \int_f \mathbf{H}_h^1 \cdot \mathbf{n}^2 \times \tilde{\pi}_f \pi^2 \mathbf{E}_h^2 \, dS \, dt + \frac{1}{2} \int_{\mathcal{I}_n} \int_f \mathbf{H}_h^2 \cdot \mathbf{n}^2 \times \pi^2 \mathbf{E}_h^2 \, dS \, dt \\
& - \frac{1}{2} \int_{\mathcal{I}_n} \int_f \pi^1 \mathbf{H}_h^1 \cdot \mathbf{n}^1 \times \mathbf{E}_h^1 \, dS \, dt - \frac{1}{2} \int_{\mathcal{I}_n} \int_f \tilde{\pi}_f \pi^1 \mathbf{H}_h^1 \cdot \mathbf{n}^2 \times \mathbf{E}_h^2 \, dS \, dt \\
& - \frac{1}{2} \int_{\mathcal{I}_n} \int_f \tilde{\pi}_f \pi^2 \mathbf{H}_h^2 \cdot \mathbf{n}^1 \times \mathbf{E}_h^1 \, dS \, dt - \frac{1}{2} \int_{\mathcal{I}_n} \int_f \pi^2 \mathbf{H}_h^2 \cdot \mathbf{n}^2 \times \mathbf{E}_h^2 \, dS \, dt \tag{26} \\
& = T_1 + T_2 + T_3 + T_4 + T_5 + T_6 + T_7 + T_8,
\end{aligned}$$

with  $\pi^1$  and  $\pi^2$  as in (15). Comparing (26) with the corresponding terms in the non-stabilized case (15), we observe, that the non-coupling terms are identical, leading to  $T_1 + T_5 = 0$  and  $T_4 + T_8 = 0$ . Only the coupling terms, are modified due to the stabilization form.

We have

$$T_2 = \frac{1}{2} \int_{\mathcal{I}_n} \int_f \mathbf{H}_h^2 \cdot \mathbf{n}^1 \times \tilde{\pi}_f \pi^1 \mathbf{E}_h^1 \, dS \, dt = \frac{1}{2} \int_{\mathcal{I}_n} \int_f \tilde{\pi}_f \mathbf{H}_h^2 \cdot \mathbf{n}^1 \times \mathbf{E}_h^1 \, dS \, dt$$

and  $\pi^1 \tilde{\pi}_f \mathbf{H}_h^2 = \tilde{\pi}_f \mathbf{H}_h^2$ , since the temporal part of  $\tilde{\pi}_f \mathbf{H}_h^2$  belongs to  $T_{K^1}(\mathcal{I}_n)$ .

Further, again using the symmetry of  $\tilde{\pi}_f$  and  $\pi^2$  we obtain

$$T_7 = -\frac{1}{2} \int_{\mathcal{I}_n} \int_f \tilde{\pi}_f \pi \mathbf{H}_h^2 \cdot \mathbf{n}^1 \times \mathbf{E}_h^1 \, dS \, dt = -\frac{1}{2} \int_{\mathcal{I}_n} \int_f \tilde{\pi}_f \mathbf{H}_h^2 \cdot \mathbf{n}^1 \times \mathbf{E}_h^1 \, dS \, dt,$$

and thus  $T_2 + T_7 = 0$ . Analogously we obtain  $T_3 + T_6 = 0$ .  $\square$

#### 4.2. A remark regarding dissipative stabilization

The problem (23) can also be augmented with an dissipative stabilization term, to obtain an upwind-type formulation (see [3], [15]). This is in particular advantageous for problems with strong singularities, or when parts of the solution can be kept under-resolved. In this case, the additional stabilization term is given by

$$\begin{aligned} D_h(\mathbf{U}_h, \mathbf{V}) &:= \int_{\mathcal{I}_n} \int_{\mathcal{F}_0} \alpha_E [\mathbf{E}_h]_T \cdot [\tilde{\pi} \mathbf{v}]_T \, dS \, dt + \int_{\mathcal{I}_n} \int_{\mathcal{F}_b} \alpha_E [\mathbf{E}_h - \mathbf{g}]_T \cdot [\mathbf{v}]_T \, dS \, dt \\ &\quad \int_{\mathcal{I}_n} \int_{\mathcal{F}_0} \alpha_H [\mathbf{H}_h]_T \cdot [\tilde{\pi} \mathbf{w}]_T \, dS \, dt, \\ \alpha_E &= c \{ \sqrt{\mu/\varepsilon} \}^{-1}, \quad \alpha_H = c \{ \sqrt{\varepsilon/\mu} \}^{-1}, \quad c \geq 0. \end{aligned}$$

However, this comes at the cost of adding dissipation to the problem. Again assuming element-wise constant material parameters  $\varepsilon, \mu$ , we obtain

$$\begin{aligned} \mathcal{E}(t_{n+1}) - \mathcal{E}(t_n) &= \int_{\mathcal{I}_n} \int_{\Omega} \mathbf{J} \cdot \pi \mathbf{E}_h \, dx \, dt - \int_{\mathcal{I}_n} \int_{\mathcal{F}_b} \mathbf{n} \times \mathbf{g} \cdot \pi \mathbf{H}_h \, dS \, dt \\ &\quad - \int_{\mathcal{I}_n} \int_{\mathcal{F}_0} \alpha_E [\tilde{\pi} \mathbf{E}_h]_T \cdot [\tilde{\pi} \mathbf{E}_h]_T \, dS \, dt - \int_{\mathcal{I}_n} \int_{\mathcal{F}_b} \alpha_E [\mathbf{E}_h - \mathbf{g}]_T \cdot [\mathbf{E}_h]_T \, dS \, dt \\ &\quad - \int_{\mathcal{I}_n} \int_{\mathcal{F}_0} \alpha_H [\tilde{\pi} \mathbf{H}_h]_T \cdot [\tilde{\pi} \mathbf{H}_h]_T \, dS \, dt, \end{aligned}$$

where the last three terms on the right-hand side are characteristic for the dissipative formulation.

## 5. Implementation

For each time slab, (10) yields a linear system of equations. Since especially for three-dimensional problems, the direct solution becomes unfeasible due to the large number of unknowns and high memory demands of sparse direct solvers, we resort to an iterative solution of (10). Rather than assembling a matrix we implement the evaluation of the residual

$$R_h(\mathbf{V}) = B_h(\mathbf{U}_h, \mathbf{V}) - L(\mathbf{V}) \tag{27}$$

directly. This is in particular advantageous in the context of adaptivity, where the discretization may change from time slab to time slab.

Furthermore under the assumptions of Theorem 3.2, we can derive a guaranteed

error bound on the iteration error. This allows to balance discretization and iteration error, leading to greatly reduced computational costs. The resulting method will, from the computational point of view behave similarly as explicit methods.

### 5.1. Basis functions for trial- and test-space

In order to allow for the efficient evaluation of the residual, we chose the tensor product basis functions

$$\hat{\mathbf{v}}_{cijkl} = l_i\left(\frac{t-t_k}{|I_k^K|}\right)\varphi_{cijkl}(\hat{x}, \hat{y}, \hat{z}) \quad (28)$$

$$\begin{aligned} \varphi_{cijkl}(\hat{x}, \hat{y}, \hat{z}) &= L_j(\hat{x})L_k(\hat{y})L_l(\hat{z})\mathbf{e}_c \\ i &= 0, \dots, p_t, \quad j = 0, \dots, p_x, \quad k = 0, \dots, p_y, \quad l = 0, \dots, p_z \end{aligned} \quad (29)$$

for the local space  $V_{h, \hat{K}}^k$ . Here  $L_i(\xi)$   $i = 0, \dots, p$  denote the orthonormal Legendre polynomials on  $[0, 1]$  and  $l_i(t)$ , the integrated Legendre polynomials on  $[0, 1]$ :

$$l_0(\xi) = 1 - \xi, \quad l_1(\xi) = \xi, \quad l_i(\xi) = \int_0^\xi L_{i-1}(s)ds \quad i = 2, \dots, p$$

Thus, the approximate solution in space-time element  $I_k^K \times K$  can be expanded as  $\mathbf{E}_h|_{I_k^K \times K} = DF^{-T}\hat{\mathbf{v}}_{cijkl}e_{cijkl}$ , where  $e_{cijkl}$  denotes the coefficients.

For the local test-spaces  $W_{h, \hat{K}}^k$  the basis is chosen to consist entirely of Legendre polynomials

$$\hat{\mathbf{w}}_{cijkl} = L_i\left(\frac{t-t_k}{|I_k^K|}\right)\varphi_{cijkl}(\hat{x}, \hat{y}, \hat{z}) \quad (30)$$

$$\begin{aligned} \varphi_{cijkl}(\hat{x}, \hat{y}, \hat{z}) &= L_j(\hat{x})L_k(\hat{y})L_l(\hat{z})\mathbf{e}_c \\ i &= 0, \dots, p_t - 1, \quad j = 0, \dots, p_x, \quad k = 0, \dots, p_y, \quad l = 0, \dots, p_z. \end{aligned} \quad (31)$$

### 5.2. Efficient evaluation of the space-time residual

In the following, we outline how the above choices of basis for the trial and test spaces lead to an efficient evaluation of the space-time residual (27). In particular, for each space-time element, the residual can be evaluated with optimal complexity of  $\mathcal{O}(p^4)$  operations in the case of affine elements and elementwise constant  $\varepsilon, \mu$  and  $\mathcal{O}(p^5)$  operations for non-affine elements, where for simplicity, in the complexity analysis, we assume isotropic polynomial degrees  $p_t = p_x = p_y = p_z$ . In the following section we use index notation and summation convention.

*Mass residual containing time derivatives*

Because of the tensor product structure of the local basis functions we can factor the space-time integral as follows

$$\begin{aligned}
R_E^{mass}(\mathbf{v}) &= \int_{I_k^K} \int_K \varepsilon \partial_t \mathbf{E}_h \cdot \mathbf{v} \, dx \, dt = \int_{I_k^K} \int_K \varepsilon \partial_t DF^{-T} \hat{\mathbf{v}}_{cijkl} \cdot DF^{-T} \hat{\mathbf{v}}_{dmnpq} \, dx \, dt e_{dmnpq} \\
&= \int_{I_k^K} L_i(\xi) \partial_t l_m(\xi) d\xi \mathcal{M}_{cijkl, dnpq} e_{dmnpq}, \\
\mathcal{M}_{cijkl, dnpq}^e &= \int_{\hat{K}} \varepsilon DF^{-T} \varphi_{cijkl}(\hat{x}, \hat{y}, \hat{z}) DF^{-T} \varphi_{dmnpq}(\hat{x}, \hat{y}, \hat{z}) |J| d\hat{x} d\hat{y} d\hat{z}
\end{aligned}$$

Note, that we have  $\int_0^1 L_i(\xi) \partial_t l_m(\xi) d\xi = \delta_{im}$  for  $i > 1, m > 1$  due to (30) and the orthogonality of the Legendre polynomials. Thus, evaluating the time derivative term corresponds to applying a spatial mass matrix  $\mathcal{M}_{cijkl, dnpq}$   $\mathcal{O}(p_t)$  times. Each application of  $\mathcal{M}_{cijkl, dnpq}$  can be done with  $\mathcal{O}(p^3)$  operations for affine and  $\mathcal{O}(p^4)$  operations for non-affine elements using fast summation techniques [16], leading to a complexity of  $\mathcal{O}(p^4)$  and  $\mathcal{O}(p^5)$  respectively.

*Curl residual*

$$\begin{aligned}
R_H^{curl}(\mathbf{v}) &= \int_{I_k^K} \int_K \nabla \times \mathbf{E}_h \cdot \mathbf{v} \, dx \, dt \quad R_{dmnpq}^{curl} = \int_{I_k^K} L_i(\xi) l_m(\xi) d\xi \mathcal{C}_{cijkl, dnpq}^{vol} e_{dmnpq} \\
\mathcal{C}_{cijkl, dnpq}^{vol} &= \int_{\hat{K}} \varphi_{cijkl}(\hat{x}, \hat{y}, \hat{z}) \cdot \nabla \times \varphi_{dmnpq}(\hat{x}, \hat{y}, \hat{z}) d\hat{x} d\hat{y} d\hat{z}
\end{aligned}$$

Here, we also have linear complexity in  $p_t$  for the number of volume-curl evaluations, since for  $m > 2$  there holds  $l_m(\xi) = (L_{m+1}(\xi) - L_{m-1}(\xi)) / \sqrt{(2m+1)}$ . Note that the curl can also be evaluated with  $\mathcal{O}(p^3)$  operations using recurrence relations for the derivatives of the Legendre polynomials (see e.g. [17]), such that a total complexity of  $\mathcal{O}(p^4)$  is obtained.

*Flux terms*

The flux terms are evaluated using fast summation techniques, such that in total  $\mathcal{O}(p^4)$  operations are needed. For two space-time elements  $I^1 \times K^1, I^2 \times K^2$  sharing the face  $f_t \times f_s, f_t = I^1 \cap I^2, f_s = \partial K^1 \cap \partial K^2$ , we consider the evaluation of the flux involving neighbor coupling. Note, that in particular we allow for nonconforming interfaces in space and time. Recalling that we have  $K^i = F_i([0, 1]^3), I^i = \tau_i([0, 1])$  and we use a co-variant transform for the spatial variables, we can write

$$\begin{aligned}
R_H^{flux}(\mathbf{v}) &= \int_{f_t} \int_{f_s} \mathbf{E}_h^2 \cdot (\mathbf{n}^1 \times \tilde{\pi}_f \mathbf{v}^1) \, dS \, dt = \\
&\int_{\tau_1^{-1}(f_t)} \int_{F_1^{-1}(f_s)} DF_1^T DF_2^{-T} \circ \psi_1^2 \hat{\mathbf{E}}_h^2 \circ \psi_1^2 \cdot (\hat{\mathbf{n}}^1 \times \tilde{\pi}_f \hat{\mathbf{v}}^1) \, d\hat{x} \, d\hat{y} \, d\hat{t}. \quad (32)
\end{aligned}$$



Here  $\psi_1^2 : \tau_1^{-1}(I^1) \times F_1^{-1}(f_s) \rightarrow \tau_2^{-1}(I^2) \times F_2^{-1}(f_s)$  is the mapping from the reference coordinates of  $I^1 \times K^1$  to those of  $I^2 \times K^2$ . The mappings  $\psi_1^2$  and  $DF_1^T DF_2^{-T}$  are constant [5] and in general affine linear with a scaled permutation matrix. Note, that the scaling part is different from the identity matrix for nonconforming interfaces only. Permutations in the spatial reference coordinates occur for general hexahedral meshes. However, for simplicity, we assume in the following that  $\psi_1^2$  is of the form  $(\hat{x}^2, \hat{y}^2, \hat{z}^2, \hat{t}^2) = (s_x \hat{x}^1 + b_x, s_y \hat{y}^1 + b_y, s_z \hat{z}^1 + b_t, s_t \hat{t}^1 + b_t)$ , i.e. no coordinate permutations are present. We have for a face with (reference) normal  $\hat{\mathbf{n}}^1 = \mathbf{e}_3$

$$\hat{\mathbf{e}}_h^2 = l_i(\hat{t})L_j(\hat{x})L_k(\hat{y})L_l(-1)e_{cijkl}\mathbf{e}_c = l_i(\hat{t})L_j(\hat{x})L_k(\hat{y})e_{c_jkl}^F\mathbf{e}_c. \quad (33)$$

Obviously,  $e_{cijkl}^F = L_l(-1)e_{cijkl}$  can be computed with  $\mathcal{O}(p^4)$  operations. With  $I_{\hat{t}} = \tau_1^{-1}(f_t)$  and  $I_{\hat{x}} \times I_{\hat{y}} = F_1^{-1}(f_s)$ , using the tensor-product structure of the trial and testspace basis functions  $\hat{\mathbf{v}}_{cijkl}$  and  $\hat{\mathbf{w}}_{dmnop}$  respectively, (32) can be written as

$$\begin{aligned} R_{dmnop}^{flux} &= L_p(1)[\tilde{\pi}_f]_{mq} \int_{I_{\hat{t}}} l_i(s_t \hat{t}^1 + b_t)L_q(\hat{t}^1) d\hat{t}^1 \int_{I_{\hat{x}}} L_j(s_x \hat{x}^1 + b_x)L_n(\hat{x}^1) d\hat{x}^1 \\ &\times \int_{I_{\hat{y}}} L_k(s_y \hat{y}^1 + b_y)L_o(\hat{y}^1) d\hat{y}^1 (\hat{\mathbf{n}}^1 \times \mathbf{e}_d) \cdot \mathbf{e}_c e_{cijkl}^F. \end{aligned}$$

Thus, the flux-residual  $R_{dmnop}^{flux}$  can be evaluated as

$$\begin{aligned} Aux1_{doij} &= \int_{I_{\hat{y}}} L_k(s_y \hat{y}^1 + b_y)L_o(\hat{y}^1) d\hat{y}^1 (\hat{\mathbf{n}}^1 \times \mathbf{e}_d) \cdot \mathbf{e}_c e_{cijkl}^F \\ Aux2_{dnoi} &= \int_{I_{\hat{x}}} L_j(s_x \hat{x}^1 + b_x)L_n(\hat{x}^1) d\hat{x}^1 Aux1_{doij} \\ Aux3_{dmno} &= [\tilde{\pi}_f]_{mq} \int_{I_{\hat{t}}} l_i(s_t \hat{t}^1 + b_t)L_q(\hat{t}^1) d\hat{t}^1 Aux2_{dnoi} \\ R_{dmnop}^{flux} &= L_p(1)Aux3_{dmno}. \end{aligned} \quad (34)$$

The complexity of each summation in (34) is  $\mathcal{O}(p^4)$ , in the case of a nonconforming interface in the respective direction. If in contrast the interface is conforming, the summation can be skipped due to the orthogonality properties of the trial and test basis functions.

In total the flux-residuals can be evaluated with  $\mathcal{O}(p^4)$  operations. Note that the same applies to non-coupling terms also.

### 5.3. Inexact iterative solution - guaranteed iteration error bound

Solving the problem exactly can be very expensive. Instead we solve the problem inexactly and control the error introduced by the inexact solution. Noting that the iteration error at solver iteration  $m$  for timeslab  $n$  fullfills

$$B_h(\mathbf{U}_h^m - \mathbf{U}_h, \mathbf{V}) = R_h^{m,n}(\mathbf{V}).$$

we can apply the stability estimate Theorem 3.2 in order to obtain the guaranteed bound on the errors  $\mathbf{e}^m = \mathbf{E}_h^m - \mathbf{E}_h$  and  $\mathbf{h}^m = \mathbf{H}_h^m - \mathbf{H}_h$  at time  $t_N$

$$\begin{aligned} \|\varepsilon^{\frac{1}{2}} \mathbf{e}^m(t_N)\|_{\mathbf{L}_2(\Omega)}^2 + \|\mu^{\frac{1}{2}} \mathbf{h}^m(t_N)\|_{\mathbf{L}_2(\Omega)}^2 &\leq 4 \sum_{n=1}^N \left( \left( \frac{2t_N}{\underline{\varepsilon}} + \frac{\Delta t^2}{2t_N \underline{\varepsilon}} \right) \|R_{h,E}^{m,n}\|_{W'_h}^2 \right. \\ &\quad \left. + \left( \frac{2t_N}{\underline{\mu}} + \frac{\Delta t^2}{2t_N \underline{\mu}} \right) \|R_{h,H}^{m,n}\|_{W'_h}^2 \right) =: \eta_{it}^2. \end{aligned} \quad (35)$$

The dual norm of the residual can be evaluated exactly by computing its Riesz-representer, which in this case, is just the application of a  $L_2$ -projection operator due to the entirely discontinuous test space.

#### 5.4. Remarks on the iterative solution procedure

Efficient preconditioning of the linear systems is currently an open problem. Nevertheless, we would like to give some remarks regarding this topic. Since the linear system governed by (23) is non-symmetric, we apply a preconditioned GMRES solver with restarting after  $n_r$  iterations, such that, denoting with  $N$  the number of degrees of freedom, the memory requirement for each timeslab is essentially  $n_r \times N$ . Usually we chose  $n_r = 10$ . As preconditioner, we apply the time-derivative terms in (23) i.e.

$$P(\mathbf{U}_h, \mathbf{V}) := \int_{\mathcal{I}_n} \int_{\Omega} \varepsilon \partial_t \mathbf{E}_h \cdot \mathbf{v} \, dx \, dt + \int_{\mathcal{I}_n} \int_{\Omega} \mu \partial_t \mathbf{H}_h \cdot \mathbf{w} \, dx \, dt. \quad (36)$$

This choice of preconditioner has the advantage, that it is in the worst-case block-diagonal with block size  $3p_x p_y p_z$ . Thus, the computational cost of one preconditioned GMRES-iteration associated with one spatial element is in terms of computational cost comparable to  $N_K$  time-steps of an explicit Runge-Kutta scheme with  $p_t$  stages. However, this simple preconditioner is effective only for sufficiently small  $\Delta t$ . This is due to the scaling with respect to  $\Delta t$  of the terms in (23) stemming from the discretization of the curl-operator.

##### 5.4.1. Example

In order to give an impression regarding the computational cost of the iterative solution process, we report the number of iterations for a  $\mathbf{T}_{mm}$ -mode in a cubic resonator in figure 3. The resonator is discretized with  $8 \times 8 \times 8$  hexahedral elements of degree  $p = p_t = p_x = p_y = p_z$ . We chose  $\Delta t = h/(2p + 1)$ , which corresponds to the maximal stable time-step reported in [18] for an SSP low-storage Runge-Kutta method of order  $p + 1$ . Further we choose the wavenumber  $m$  as 1, 2 and 3 for  $p = 1, 2, p = 3, 4$  and  $p = 5, 6$  respectively. The exact solution of the linear systems requires about  $N_{it} = 20 - 30$  iterations per time-slab. The resulting computational costs are prohibitively high, in particular when compared to a fully explicit scheme such as [18], where the cost is roughly equal to one iteration. For inexact solution, the number of iterations is reduced by a factor of 2-4.2 and is in the range of  $\tilde{N}_{it} = 4 - 9$ . Furthermore, the iteration-error bound consistently overestimates the iteration error with efficiency-index

$p$	steps	$N_{it}$	$\tilde{N}_{it}$	speedup	$e(T)$	$\tilde{e}(T)$	$I_{eff}$
1	189	7.9	4.0	2.0	$2.04 \times 10^{-1}$	$2.04 \times 10^{-1}$	1.66
2	315	24.0	6.1	4.0	$3.65 \times 10^{-3}$	$3.90 \times 10^{-3}$	3.12
3	220	25.0	6.0	4.2	$5.57 \times 10^{-3}$	$5.31 \times 10^{-3}$	6.75
4	283	20.0	7.8	2.6	$2.30 \times 10^{-4}$	$2.26 \times 10^{-4}$	12.58
5	213	22.0	8.6	2.5	$1.91 \times 10^{-4}$	$1.83 \times 10^{-4}$	5.67
6	252	18.0	8.8	2.0	$4.84 \times 10^{-5}$	$4.83 \times 10^{-5}$	5.70

Figure 3: Number of time-steps, average number of GMRES-iterations  $N_{it}$  per time-step for exact and  $\tilde{N}_{it}$  for inexact solution of the linear systems, speedup in terms of total iterations, errors  $e(T) = \|\mathbf{U}(T) - \mathbf{U}_h(T)\|_{\mathbf{L}_2(\Omega)}$  and  $\tilde{e}(T) = \|\mathbf{U}(T) - \tilde{\mathbf{U}}_h(T)\|_{\mathbf{L}_2(\Omega)}$  for exact and inexact solution and efficiency index for the iteration error bound (35)  $I_{eff} = \eta_{it} / \|\mathbf{e}_h^n(T) - \mathbf{e}_h(T)\|_{\mathbf{L}_2(\Omega)}$

$I_{eff} = 2 - 12$ , such that the total error is not increased by the inexact solution.

## 6. Numerical Experiments

The first two numerical experiments feature basic academic examples for assessing convergence properties when local refinement, especially with respect to time, is present in the discretization.

### 6.1. Convergence tests on non-adaptive discretizations

#### 6.1.1. TM Mode hp-discretization

The initial data is chosen such that the  $\text{TM}_{mn}$  mode is approximated in  $\Omega = [0, 1] \times [0, 1] \times [0, 1/5]$ . We choose  $m = n = 1$  leading to frequency  $\omega = \pi\sqrt{m^2 + n^2}$ . The exact solution for the electric field is:

$$\mathbf{E} = \sin(m\pi x) \sin(n\pi y) \cos(\omega t) \mathbf{e}_z \quad (37)$$

The time traces of the spatial  $L_2$ -error are depicted for 200 periods of the solution in Fig. 5. Furthermore, in Fig. 5 one can observe exponential convergence in the norm  $\|\cdot\|_{L_2(\mathcal{I}_n; \mathbf{L}_2(\Omega))}$ .

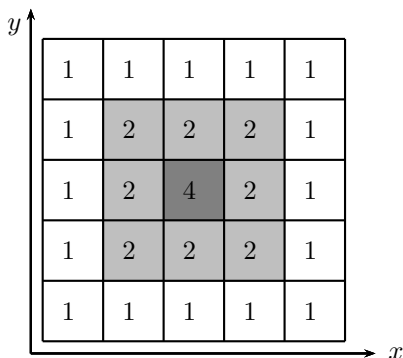


Figure 4: The spatial mesh. Numbers inside elements denote the number of local time steps. The polynomial degrees are chosen isotropically (in space and time), and increase from  $p = p_{min}$  to  $p = p_{min} + 2$  from the boundary to the center of the computational domain according to the shading.

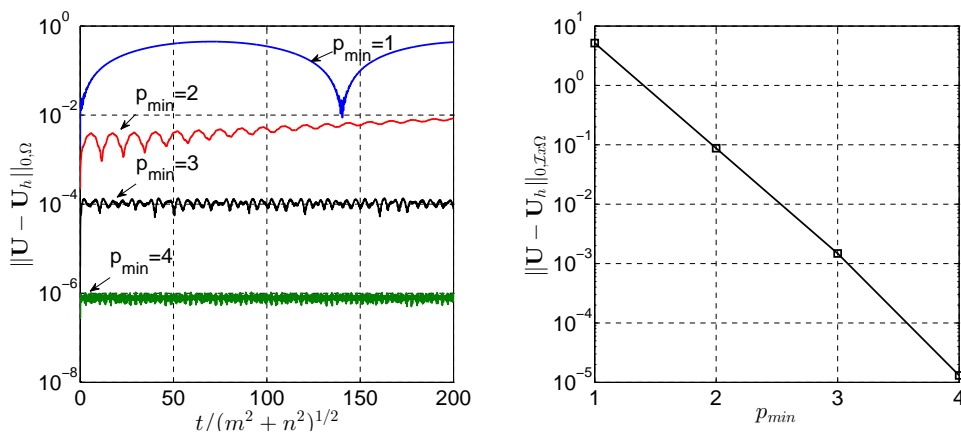


Figure 5: Left: Temporal evolution of the spatial  $L_2$ -error, right: error  $\|\mathbf{U} - \mathbf{U}_h\|_{L_2(\mathcal{I}; L_2(\Omega))}$  for  $p_{min} = 1, 2, 3, 4$  and the setup depicted in Fig. 4

### 6.1.2. Local $h$ -refinement in time

In order to exploit the temporal accuracy of the method in the case of local  $h$ -refinement in time direction, the source term and boundary conditions are chosen such that the exact solution [19] is

$$\begin{aligned} \mathbf{E} &= e^t x(x-1)z(1-z)\mathbf{e}_y, \\ \mathbf{H} &= e^t x(x-1)(1-2z)\mathbf{e}_x - e^t(2x-1)z(1-z)\mathbf{e}_z. \end{aligned}$$

The problem is solved on the space-time domain  $\mathcal{I} \times \Omega$  with  $\mathcal{I} = [0, 5]$ ,  $\Omega = [0, 1]^3$ , which is subdivided in time slabs  $\Delta t \times \Omega$ . The spatial mesh and the temporal refinement level associated with each spatial cell is shown in Fig. 6. The solution

is approximated with quadratic polynomials in the  $x - z$  directions, such that the temporal error is expected to be dominating. In the temporal direction the polynomial degree is set to  $p_t$ . In Fig. 7 left, one can observe that the error in the norm  $\|\cdot\|_{L_2(\mathcal{I};\mathbf{L}_2(\Omega))}$  is of order  $p_t + 1$ . If we instead consider the quantity  $\max_k \|\mathbf{U}(t_k) - \mathbf{U}_h(t_k)\|_{\mathbf{L}_2(\Omega)}$ , an order of  $2p_t$  can be observed in Fig. 7 right. For continuous-Galerkin (cG) time stepping schemes, this nodal superconvergence behaviour is reported in [20].

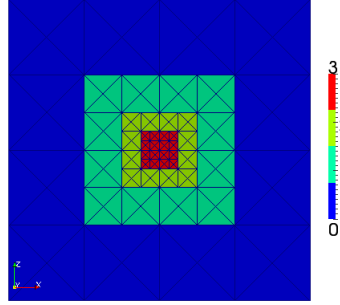


Figure 6: Temporal refinement level

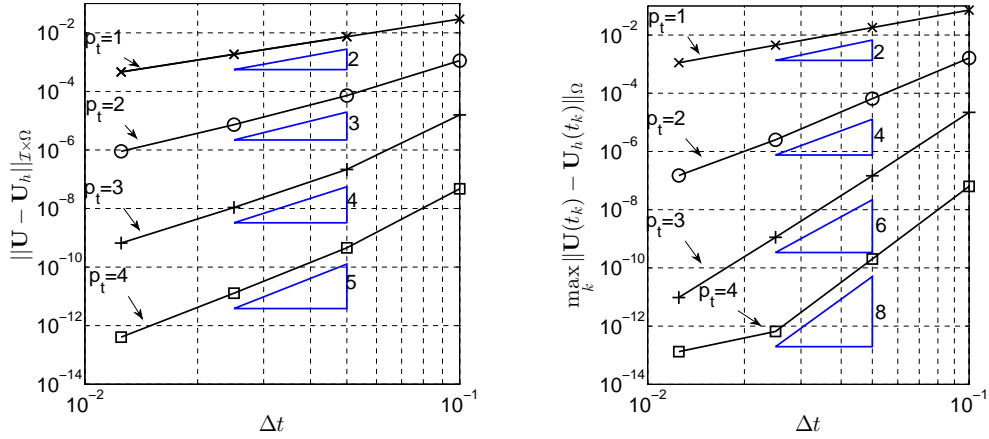


Figure 7: Left: error  $\|\mathbf{U} - \mathbf{U}_h\|_{L_2(\mathcal{I};\mathbf{L}_2(\Omega))}$ , right: error  $\max_k \|\mathbf{U}(t_k) - \mathbf{U}_h(t_k)\|_{0,\Omega}$  for the local  $h$ -refinement with respect to time depicted in Fig.6

### 6.1.3. Broadband pulse in a waveguide

We consider a broadband pulse in a coaxial waveguide. The exact solution is

$$\begin{aligned}\mathbf{E} &= \frac{1}{r} e^{-(\pi(f_2-f_1)(z-t)/2)^2} \sin(\pi(f_1+f_2)(z-t)) \mathbf{e}_r \\ \mathbf{H} &= \frac{1}{r} e^{-(\pi(f_2-f_1)(z-t)/2)^2} \sin(\pi(f_1+f_2)(z-t)) \mathbf{e}_\varphi.\end{aligned}$$

Here  $r$ ,  $\varphi$  and  $z$  denote the radial, azimuthal and axial coordinates respectively and  $\mathbf{e}_r$ ,  $\mathbf{e}_\varphi$  and  $\mathbf{e}_z$  the corresponding unit vectors. The mid-frequency  $(f_1+f_2)/2$  is chosen such that the corresponding wavelength is approximately 1/16 the length of the waveguide. The spatial mesh consists of 1600 hexahedra with an edge-length of approximately  $1/3\lambda$ . The global time step is fixed, such that in total 400 time steps are necessary to propagate the pulse through the entire waveguide. In Fig. 8 we show the time trace of the spatial  $L_2$ -errors. The error exhibits an odd even pattern, the origin of which is yet unknown. We suspect this behavior to be related to the choice of a central flux. A similar behaviour is reported in [21].

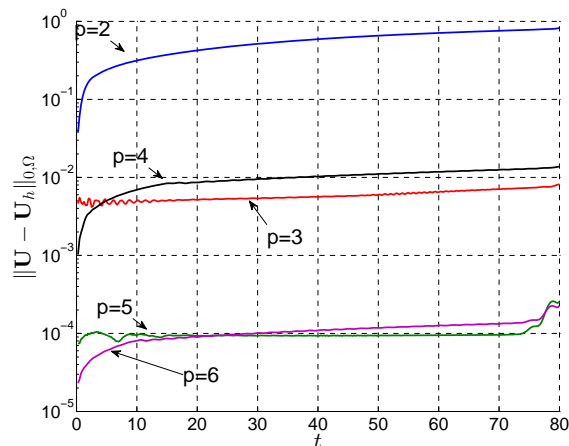


Figure 8: Temporal evolution of the spatial  $L_2$ -error for  $p = 2, 3, 4, 5, 6$

### 6.1.4. Bi-static RCS, metallic sphere - global $p$ -refinement

A metallic sphere of radius  $a = 1$  is illuminated by a  $\mathbf{e}_x$ -polarized plane wave traveling in  $e_z$ -direction with wave number  $\omega = 2\pi$ . We chose  $\Omega$  as a spherical shell with outer radius  $R = 5$ . For the outer boundary a Silver-Müller boundary condition is applied. The spatial grid consists of only 576 hexahedral elements with about 2 elements per wavelength at the surface of the scatterer and one element per wavelength at the absorbing boundary. The polynomial degrees are

chosen as  $p = p_t = p_x = p_y = p_z = p_{geo}$ , where  $p_{geo}$  is the polynomial degree of the elemental mapping  $F$ . We compute the bi-static RCS

$$\sigma(\phi, \theta) = \lim_{r \rightarrow \infty} 4\pi r^2 \frac{|\mathbf{E}_{sc}(r, \phi, \theta)|^2}{|\mathbf{E}_{inc}(r, \phi, \theta)|^2}$$

Here  $r$  denotes the distance from the center of the sphere to the point of observation  $r\mathbf{x}$ ,  $\phi$  and  $\vartheta$  the azimuthal and polar angle between the wave and  $\mathbf{x}$ . The scattered far field is evaluated at a closed surface  $S$ , one wavelength away from the scatterer by evaluating the near-to-far field transformation

$$\mathbf{E}_{sc} = \frac{e^{-i\omega r}}{4\pi r} \int_{t_0}^{t_1} \int_S [\mathbf{x} \times (\mathbf{x} \times (\mathbf{n} \times \mathbf{H}_h)) + \mathbf{x} \times (\mathbf{E}_h \times \mathbf{n})] e^{i\omega \mathbf{x} \cdot \mathbf{y} - i\omega t} dS(\mathbf{y}) dt$$

with Gauss quadrature of sufficiently high order. The computed RCS in Fig. 9 converge quickly to the analytical Mie-series solution.

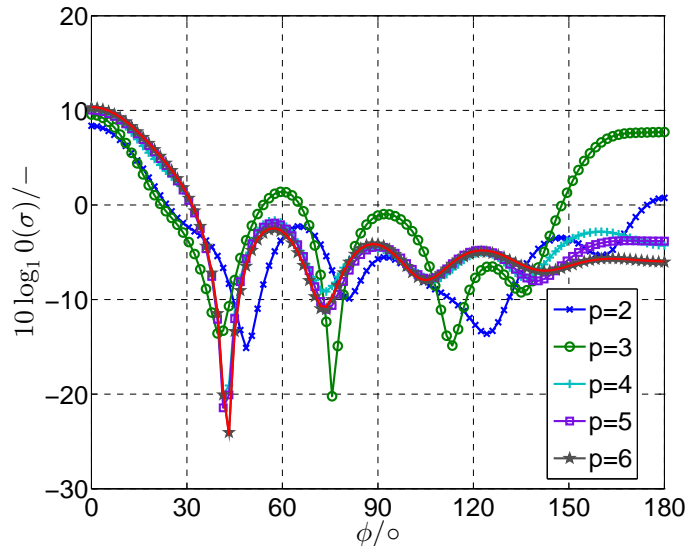


Figure 9: Bi-static RCS, of a  $ka = 2\pi$  PEC sphere, numerical solutions for a 576-element mesh with polynomial degrees  $p = 2, \dots, 6$  and the analytical Mie-series solution (red)

### 6.2. Space-time $hp$ -adaptive examples

In order to demonstrate the method's capability for space-time  $hp$ -refinement, we propose an adaptive algorithm, which extends the concept of reference solutions [7, 22] to the space-time context.

- First a global time step  $\Delta t$ , resulting in equally sized time slabs, is chosen.
- Given a time slab  $\Delta t \times \Omega$ , an initial mesh  $\mathcal{S}_0$  and polynomial-degree distribution  $\mathbf{p}_0$
- Define a coarse discretization  $(\mathcal{S}_H, \mathbf{p}_H) = (\mathcal{S}_0, \mathbf{p}_0)$  and a refined discretization  $(\mathcal{S}_h, \mathbf{p}_h)$  with finite element spaces  $V_H$  and  $V_h$  respectively. The refined discretization is obtained by isotropically refining all space-time elements and increasing the polynomial degrees by one. Note that  $V_H$  is contained in  $V_h$ .

Then the following steps are performed iteratively

1. SOLVE: Solve the problem (10) on the coarse and fine discretizations.
2. ESTIMATE: Compute the error indicators  $\eta(\mathcal{I}_n \times K) = \|\mathbf{U}_h - \mathbf{U}_H\|_{L_2(\mathcal{I}_n; \mathbf{L}_2(\Omega))}$  and the approximate error bound  $\|\mathbf{U}_h - \mathbf{U}_H\|_{L_2(\mathcal{I}_n; \mathbf{L}_2(\Omega))} \leq TOL$  stop and proceed to the next time slab. Otherwise,
3. MARK: Apply a fixed fraction marking strategy [23] based on the indicators  $\eta(\mathcal{I}_n \times K)$
4. REFINE: For each marked  $\mathcal{I}_n \times K$ , set up a list of refinement candidates  $V_{H, \mathcal{I}_n \times K}^{\text{cand}}(\mathcal{I}_n \times \hat{K}, \mathbf{p}_K)$ . In particular, we allow for all combinations of the following modifications of the discretization parameters:
  - raise/decrease the polynomial degrees  $p_x, p_y, p_z, p_t$
  - isotropically  $h$ -refine/derefine in the spatial directions
  - increase/decrease the temporal refinement level

In case of an refinement, which yields new space-time elements, we restrict the number of candidates by choosing identical polynomial degrees for each new element.

Choose

$$\begin{aligned}
V_{H, \mathcal{I}_n \times K} &= \arg \min_{V_H^{\text{cand}}, S.T. \eta - \eta^{\text{cand}} > 0} \frac{\eta^{\text{cand}} - \eta}{\#DOF(V_H^{\text{cand}})}, \eta^{\text{cand}} \\
&= \|\mathbf{U}_h - \Pi_{V_h}^{V_H^{\text{cand}}} \mathbf{U}_h\|_{L_2(\mathcal{I}_n; \mathbf{L}_2(\Omega))}^2
\end{aligned}$$

as the new local finite elements space, leading to a new global space  $V_H$ . Build a new  $V_h$  from  $V_H$  and go back to SOLVE.

- Now, for the current time slab the final coarse and fine grid solutions have been obtained.

*Remark1:* The initial data for coarse- and fine-grid solves for the current time slab is taken as the  $L_2$ -projection of the refined solution  $U_h$  from the previous time slab. Note that in the case of spatial derefinement with respect to the previous time slab, i.e. if the spatial part of the finite element space is not contained in the current one, there will be dissipation introduced by the projection. See [24], for a more detailed discussion. However the amount of dissipation introduced seemed to be negligible compared to the total error for the examples



we have considered.

*Remark2:* If an iterative solver is applied, we can choose the coarse grid solution as starting point for solving the fine grid problem. We have observed, that this considerably cuts down the number of fine grid iterations.

### 6.2.1. Broadband pulse in coaxial waveguide

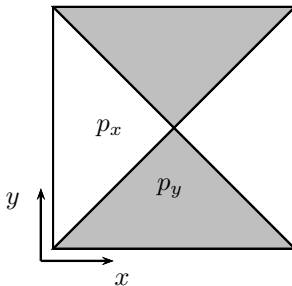


Figure 10: Visualization of tensor product polynomials with degrees  $p_x, p_y$

We have solved the example from 6.1.3 with the  $hp$ -adaptive algorithm. For the initial discretization we have chosen a coarse mesh consisting of 200 elements of degree  $p_t = 1, p_x = p_y = p_z = 0$ . In Fig. 11 we visualize the coarse grid  $hp$ -discretization for time slab 86, by showing from top to bottom the electric field magnitude, the spatial polynomial discretization, using the tensor product visualization depicted in Fig. 10 and the temporal polynomial degree distribution. In axial direction, where the pulse has greater variation, spatial polynomial degrees are chosen to be larger than in radial direction. The temporal polynomial degrees are raised in the area where the pulse is situated. The temporal refinement level was not raised in any of the time slabs. For the  $hp$ -adaptive solution we have obtained a relative fine-grid error in the norm  $\|\cdot\|_{L_2(\cdot; L_2(\Omega))}$  of  $9.6e - 3$ .

### 6.2.2. Scattering of a dielectric sphere

In the following, we consider the scattering of a Gaussian plane-wave by a dielectric sphere with  $\varepsilon = 4$ . The problem again was solved using the  $hp$ -adaptive algorithm. For the initial discretization we have chosen a coarse mesh consisting of 72 elements of degree  $p_t = 1, p_x = p_y = p_z = 0$ . The discretization of time slabs 33, 65 and 124 (from top to bottom) is depicted in Fig. 12. The fact that the electric field has limited regularity at the material interface is reflected by the choice of moderate polynomial degrees in space and linear polynomial degrees in time and a comparatively small spatial mesh size near the material interface. Refinement in the temporal direction was almost exclusively  $h$ -refinement, i.e. the temporal polynomial degree was almost exclusively equal

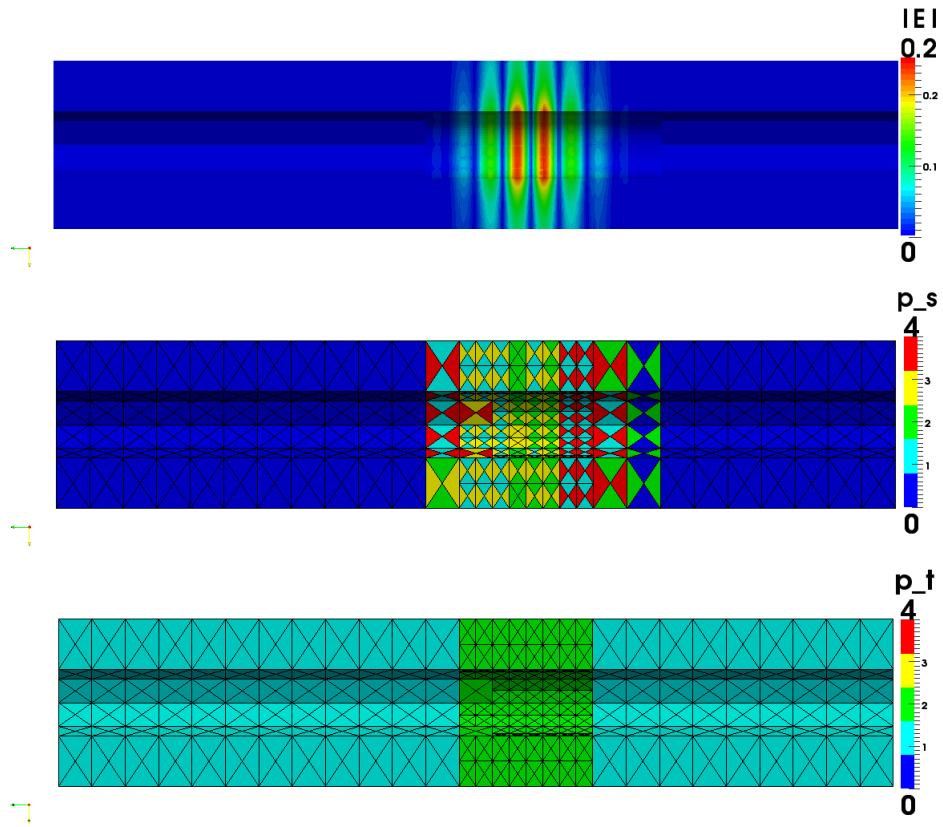


Figure 11: Propagation of a broadband pulse in a cylindrical waveguide. From top to bottom: distribution of  $|\mathbf{E}_h|$ ,  $(p_x, p_y, p_z)$ , and  $p_t$

to one. Thus we do not show the temporal polynomial degree distributions. The bi-static RCS for  $ka = 1$  is depicted in Fig. 13, where a relative  $\ell_2$ -error of  $2.53 \cdot 10^{-2}$  was obtained.

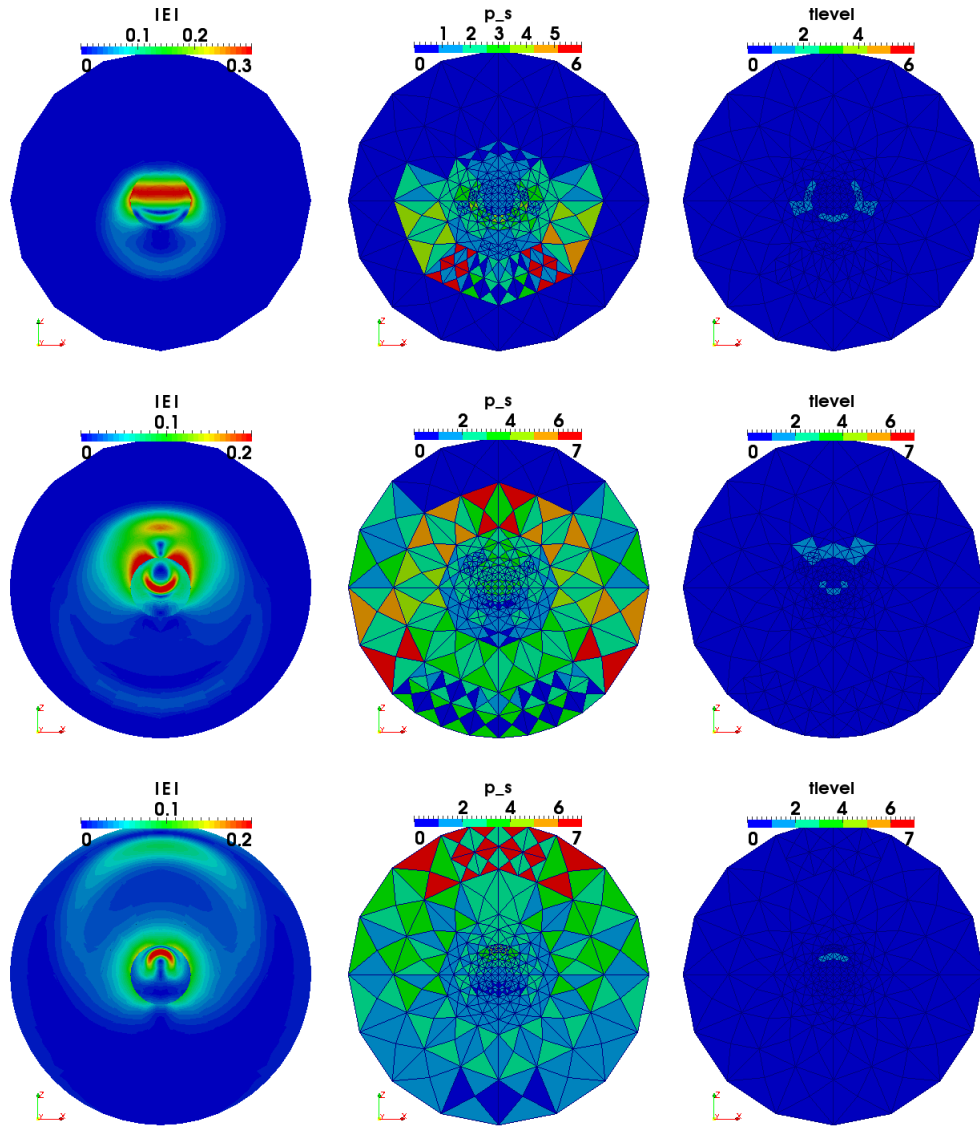


Figure 12:  $hp$ -adaptive simulation of the scattering from a dielectric sphere. From left to right: distribution of  $|\mathbf{E}_h|$ , spatial polynomial degrees  $(p_x, p_y, p_z)$  and temporal refinement level at timeslab 34, 66, 125 (from top to bottom)

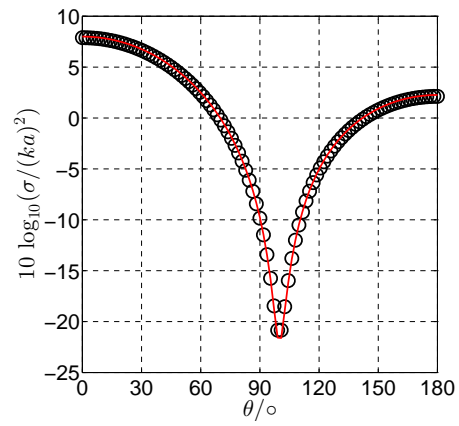


Figure 13: Bistatic RCS of a dielectric sphere with  $\varepsilon = 4$  and  $ka=1$ , numerical solution (black circles), analytical Mie-series solution (red line)

## 7. Conclusions

We have devised a space-time Galerkin method, which allows for local *hp*-refinement in space and time by treating the spatial part of the discretization with a DG approach, whereas the temporal part is treated with a continuous Galerkin approach. The resulting implicit method can be shown to be non-dissipative, as long as the spatial part of the discretization is kept constant from time-slab to time-slab. We have shown, that the method can be implemented, such that the complexity of the residual evaluation for an iterative solution is  $\mathcal{O}(p^4)$  for affine elements and  $\mathcal{O}(p^5)$  for non affine elements. Furthermore, for the case of no local refinement with respect to time, we have devised an *a posteriori* bound on the iteration error. Thus a balancing of the iteration and discretization errors is possible, provided that an *a posteriori* estimate for the discretization error is available. While the presented method has higher computational costs than explicit hp-DG methods such as [24, 25], it provides the possibility to apply hp-adaptivity not only in space but also in time. It therefore allows to control the approximation error in the entire space-time domain of interest. We presented numerical experiments confirming that the method can be used for fully space-time hp-adaptive simulations.

The *a priori* and *a posteriori* error analysis is subject of ongoing work. Other future work should relate to the investigation of more efficient methods for the iterative solution of the linear systems, in particular regarding preconditioning.

## References

### References

- [1] J. Van der Vegt, H. Van der Ven, Space-time discontinuous galerkin finite element method with dynamic grid motion for inviscid compressible flows: I. general formulation, *Journal of Computational Physics* 182 (2) (2002) 546–585.
- [2] C. Schwab, *p-and hp-Finite Element Methods: Theory and Applications to Solid and Fluid Mechanics*, Oxford University Press, USA, 1999.
- [3] J. Hesthaven, T. Warburton, Nodal high-order methods on unstructured grids, *Journal of Computational Physics* 181 (1) (2002) 186–221. doi:10.1006/jcph.2002.7118. URL <http://linkinghub.elsevier.com/retrieve/pii/S0021999102971184>
- [4] L. Fezoui, S. Lanteri, S. Lohrengel, S. Piperno, Convergence and stability of a discontinuous galerkin time-domain method for the 3D heterogeneous maxwell equations on unstructured meshes, *ESAIM: Mathematical Modelling and Numerical Analysis* 39 (6) (2005) 1149–1176. doi:10.1051/m2an:2005049. URL <http://www.esaim-m2an.org/10.1051/m2an:2005049>

- [5] G. Cohen, X. Ferrieres, S. Pernet, A spatial high-order hexahedral discontinuous galerkin method to solve maxwells equations in time domain, *Journal of Computational Physics* 217 (2) (2006) 340–363. doi:10.1016/j.jcp.2006.01.004.  
URL <http://linkinghub.elsevier.com/retrieve/pii/S0021999106000131>
- [6] L. Demkowicz, *Computing with Hp-adaptive Finite Elements: One and two dimensional elliptic and Maxwell problems*, Vol. 1, CRC Press, 2006.
- [7] L. Demkowicz, J. Kurtz, D. Pardo, M. Paszenski, W. Rachowicz, A. Zdunek, *Computing with hp-ADAPTIVE FINITE ELEMENTS: Volume II Frontiers: Three Dimensional Elliptic and Maxwell Problems with Applications*, Vol. 2, Chapman & Hall/CRC, 2007.
- [8] S. Piperno, Symplectic local time-stepping in non-dissipative DGTD methods applied to wave propagation problems, *ESAIM: Mathematical Modelling and Numerical Analysis* 40 (05) (2006) 815–841.
- [9] A. Taube, M. Dumbser, C.-D. Munz, R. Schneider, A high-order discontinuous galerkin method with time-accurate local time stepping for the maxwell equations, *International Journal of Numerical Modelling: Electronic Networks, Devices and Fields* 22 (1) (2009) 77–103.
- [10] V. Dolean, H. Fahs, L. Fezoui, S. Lanteri, Locally implicit discontinuous galerkin method for time domain electromagnetics, *Journal of Computational Physics* 229 (2) (2010) 512–526. doi:10.1016/j.jcp.2009.09.038.  
URL <http://linkinghub.elsevier.com/retrieve/pii/S0021999109005300>
- [11] S. Descombes, S. Lanteri, L. Moya, Locally implicit time integration strategies in a discontinuous galerkin method for maxwells equations, *Journal of Scientific Computing* (2012) 1–29doi:10.1007/s10915-012-9669-5.  
URL <http://dx.doi.org/10.1007/s10915-012-9669-5>
- [12] R. Griesmaier, P. Monk, Discretization of the wave equation using continuous elements in time and a hybridizable discontinuous galerkin method in space, *Journal of Scientific Computing* (2013) 1–27doi:10.1007/s10915-013-9741-9.  
URL <http://dx.doi.org/10.1007/s10915-013-9741-9>
- [13] M. Remaki, *Mthodes numriques pour les quations de maxwell instationnaires en milieu htrogne*, Ph.D. thesis, Ecole des Ponts ParisTech (1999).
- [14] J. Jackson, *Classical electrodynamics*, *Classical Electrodynamics*, 3rd Edition, by John David Jackson, pp. 832. ISBN 0-471-30932-X. Wiley-VCH, July 1998. 1.
- [15] E. Montseny, S. Pernet, X. Ferrires, G. Cohen, Dissipative terms and local time-stepping improvements in a spatial high order discontinuous galerkin scheme for the time-domain maxwells equations, *Journal of Computational*

Physics 227 (14) (2008) 6795–6820. doi:10.1016/j.jcp.2008.03.032.  
URL <http://linkinghub.elsevier.com/retrieve/pii/S0021999108001836>

- [16] J. Melenk, K. Gerdes, C. Schwab, Fully discrete *hp*-finite elements: fast quadrature, Computer methods in applied mechanics and engineering 190 (32) (2001) 4339–4364.
- [17] C. Koutschan, C. Lehrenfeld, J. Schöberl, Computer algebra meets finite elements: An efficient implementation for maxwells equations, Numerical and Symbolic Scientific Computing: Progress and Prospects 1 (2011) 105.
- [18] D. Srmny, M. Botchev, J. J. van der Vegt, Dispersion and dissipation error in high-order runge-kutta discontinuous galerkin discretisations of the maxwell equations, Journal of Scientific Computing 33 (1) (2007) 4774.
- [19] J. G. Verwer, Composition methods, maxwell’s equations, and source terms, SIAM Journal on Numerical Analysis 50 (2) (2012) 439–457. doi:10.1137/100816122.  
URL <http://epubs.siam.org/doi/abs/10.1137/100816122>
- [20] G. Akrivis, C. Makridakis, R. H. Nochetto, Galerkin and RungeKutta methods: unified formulation, a posteriori error estimates and nodal superconvergence, Numerische Mathematik 118 (3) (2011) 429–456.
- [21] J. S. Hesthaven, T. Warburton, Nodal discontinuous Galerkin methods: algorithms, analysis, and applications, Vol. 54, Springer, 2007.
- [22] P. Solin, K. Segeth, I. Dolezel, Higher-order finite element methods, Vol. 41, Chapman and Hall/CRC, 2003.
- [23] W. Dörfler, A convergent adaptive algorithm for poisson’s equation, SIAM Journal on Numerical Analysis 33 (3) (1996) 1106–1124.
- [24] S. Schnepf, T. Weiland, Efficient large scale electromagnetic simulations using dynamically adapted meshes with the discontinuous galerkin method, Journal of Computational and Applied Mathematics (2012) 4909–4924.
- [25] S. M. Schnepf, Error-driven dynamical *hp*-meshes for the discontinuous galerkin method in time-domain, Journal of Computational and Applied Mathematics 270 (2014) 353–368. doi:10.1016/j.cam.2013.12.038.  
URL <http://www.sciencedirect.com/science/article/pii/S0377042713007115>

## Acknowledgements

The work of M. Lilienthal is supported by the ‘Excellence Initiative’ of the German Federal and State Governments and the Graduate School of Computational Engineering at Technische Universität Darmstadt and the DFG under grant no. DFG WE 1239/27-2.

S.M. Schnepp acknowledges the support of the Alexander von Humboldt Foundation through a Feodor Lynen-Research Fellowship.

We thank Jens Niegemann for providing code for the computation of the Mie-series solutions.

We would like to thank Herbert Egger for giving valuable hints, which improved the presentation of the material significantly.